



The YOPP site Model Intercomparison Project (YOPPsiteMIP) phase 1: project overview and Arctic winter forecast evaluation

Jonathan J. Day¹, Gunilla Svensson², Barbara Casati³, Taneil Uttal⁴, Siri-Jodha Khalsa⁵, Eric Bazile⁶, Elena Akish⁴, Niramson Azouz⁶, Lara Ferrighi⁷, Helmut Frank⁸, Michael Gallagher^{4,9}, Øystein Godøy⁷, Leslie M. Hartten^{4,9}, Laura X. Huang³, Jareth Holt², Massimo Di Stefano⁷, Irene Suomi¹⁰, Zen Mariani³, Sara Morris⁴, Ewan O'Connor¹⁰, Roberta Pirazzini¹⁰, Teresa Remes⁷, Rostislav Fadeev¹¹, Amy Solomon^{4,9}, Johanna Tjernström¹², Mikhail Tolstykh^{11,13},

¹European Centre for Medium-Range Weather Forecasts, Reading, United Kingdom

²Department of Meteorology and Bolin Centre for Climate Change, Stockholm University, Sweden.

10 ³Meteorological Research Division, Environment and Climate Change Canada, Canada.

⁴NOAA Physical Science Laboratory, Boulder, Colorado, USA.

⁵National Snow and Ice Data Center, University of Colorado,

⁶Meteo France, Toulouse, France

⁷Norwegian Meteorological Institute, Oslo, Norway.

15 ⁸Deutscher Wetterdienst, Offenbach, Germany

⁹Cooperative Institute for Research in Environmental Science (CIRES), University of Colorado, Boulder, Colorado, USA

¹⁰Finnish Meteorological Institute, Helsinki, Finland.

¹¹Marchuk Institute of Numerical Mathematics Russian Academy of Sciences, Russia

¹²Swedish Meteorological and Hydrological Institute, Linköping, Sweden

20 ¹³Hydrometeorological Research Centre of Russia, Russia

Correspondence to: Jonathan J. Day (jonathan.day@ecmwf.int)

Abstract.

25 Although the quality of weather forecasts in the polar regions is improving, forecast skill there still lags the lower latitudes. So far there have been relatively few efforts to evaluate processes in Numerical Weather Prediction systems using in-situ and remote sensing datasets from meteorological observatories in the terrestrial Arctic and Antarctic, compared to the mid-latitudes. Progress has been limited both by the heterogeneous nature of observatory and forecast data but also by limited availability of the parameters needed to perform process-oriented evaluation in multi-model forecast archives. The YOPP site
30 Model Inter-comparison Project (YOPPsiteMIP) is addressing this gap by producing Merged Observatory Data Files (MODFs) and Merged Model Data Files (MMDFs), bringing together observations and forecast data at polar meteorological observatories in a format designed to facilitate process-oriented evaluation.

An evaluation of forecast performance was performed at seven Arctic sites, focussing on the first YOPP Special Observing
35 Period in the Northern Hemisphere (SOP1), February and March 2018. It demonstrated that although the characteristics of forecast skill vary between the different sites and systems, an underestimation in boundary layer temperature variance across models, which goes hand in hand with an inability to capture cold extremes, is a common issue at several sites. Diagnostic analysis using surface fluxes suggests that this is at least partly related to insufficient thermal representation of the land-surface in the models, which all use a single layer snow model.

40 1 Introduction

Recent decades have seen a marked increase in human activity in the polar regions leading to an increasing societal demand for weather and environmental forecasts (Emmerson and Lahn, 2012; Goessling et al., 2016). Despite this growing need, the skill of weather forecasts in the polar regions lags that of the mid-latitudes (Jung et al., 2016; Bauer et al., 2016). This is partly the result of the relatively lower density of conventional observations in high compared to mid-latitudes (Lawrence et al.,



45 2019), but is also related to the occurrence of meteorological situations and phenomena which are historically difficult to
model such as stable boundary layers (e.g. Atlaskin and Vihma, 2012; Sandu et al., 2013; Holtslag et al., 2013), mixed-phase
clouds (e.g. Pithan et al., 2014, 2016, Solomon et al., 2023), and the importance of coupling between the atmosphere and snow
and ice surfaces (e.g. Day et al., 2020; Batrak and Muller, 2019; Svensson and Karlsson, 2011).

50 The ability of climate models to represent atmospheric processes in polar regions has recently been assessed highlighting
deficiencies in near-surface and boundary layer properties (Pithan et al., 2014; Svensson and Karlsson, 2011; Karlsson and
Svensson, 2013). Since many climate models are based on global weather forecasting systems, understanding the causes of
forecast error after 1-2 days may help develop understanding of the sources of error in climate models (Rodwell and Palmer,
2007). Nevertheless, until recently there has been little focus on evaluating Numerical Weather Prediction (NWP) models
55 using in-situ data from the terrestrial Arctic and Antarctic (Jung and Matsueda, 2014; Jung et al., 2016).

Recent studies, conducted as part of the World Weather Research Programme's Polar Prediction Project (PPP, Jung et al,
2016) have started to address this gap, assessing the skill of both the large scale circulation (Bauer et al., 2016) and surface
weather properties (Køltzow et al., 2019). The Year of Polar Prediction (YOPP) site Model Intercomparison Project
60 (YOPPsiteMIP) was designed to build on these earlier studies by utilising process level data from polar observatories to
diagnose the causes of forecast error from a process perspective and ultimately inform model development. Although process-
oriented evaluation studies focussing on polar processes are not new, those that have been done have tended to focus on one
or two sites or a specific field campaign (see Day et al., 2020; Batrak and Müller, 2019; Miller et al., 2018; Tjernström et al.,
2021 for some recent examples). A key aim of YOPPsiteMIP is to provide a pan-Polar perspective on forecast evaluation and
65 process representation.

YOPPsiteMIP participants were asked to provide data in so-called Merged Data Files (MDFs) which includes both Merged
Observatory Data Files (MODFs), for observatory data, and Merged Model Data Files (MMDFs), for model data. These data
standards, which were developed specifically for YOPPsiteMIP, are described by Uttal et al. (2023). Using this common file
70 format, with consistent naming and metadata, facilitates equitable and efficient comparisons between models and observations.
This standardisation of the data from different observatories also aids interoperability in the sense that the same evaluation
code can be applied at different sites. These MDF filetypes were developed as part of PPP, following the FAIR (Findable,
Accessible, Interoperable, Reusable) data principles (Wilkinson, 2016). Details of the MDF concept and specifics of the data
processing chain and related Python toolkit for producing MDFs are described in Uttal et al. (2023) and Gallagher et al., (in
75 prep).

The observatories selected for YOPPsiteMIP represent a geographically diverse set of locations. At these sites a wide range of
instruments measuring properties of the air, snow and soil are employed, extending far beyond the traditional synoptic surface
and upper-air observation network, which are collected for use in the production and evaluation of NWP systems (Uttal et al.,
80 2015). Taken together, the observations collected at these observatories offer opportunities to develop a deeper understanding
of the physical processes governing the weather in the polar regions, their representation in forecast models, and how this
varies from site to site. The processes and phenomena targeted in YOPPsiteMIP include boundary-layer turbulence, surface
exchange (including over snow and ice) and mixed-phase clouds.

85 A benefit of organizing coordinated evaluation involving several NWP systems and multiple sites is that it helps clarify if the
issues revealed by the analysis are model or location specific. The modelling community has organized model inter-
comparisons to target various atmospheric processes relevant for Arctic conditions (e.g. Cuxart et al., 2006; Pithan et al., 2016;



Tjernström et al 2005, Sedlar et al. 2020, Solomon et al., 2023) each using its own protocol for data sharing. However, the newly developed standardisation of the observational and forecast model data developed for YOPPsiteMIP is planned to be used for future MIIPs (model intercomparison and improvement projects). Converging on a standard like this will aid interoperability, making it easier for model developers to expand their evaluation to new sites or observational campaigns, but also to other models or forecasting systems.

MMDFs were requested for the locations listed in Table 1 and shown in Figure 1 during the YOPP Special Observing Periods, during which the observations taken at many polar observatories (e.g. the frequency of radiosondes) was enhanced (see Lawrence et al., 2019; Bromwich et al., 2020). For the Northern Hemisphere the periods Feb–Mar 2018 and Jul–Sep 2018 were selected and named NH-SOP1 and SOP2 respectively. For the Southern Hemisphere or SH-SOP the period Nov–Feb 2018/19 was chosen.

Observatory name <i>Filename</i>	Latitude Longitude	Elevation
Arctic land sites		
Utqiagvik (Formerly known as Barrow, Alaska) <i>Utqiagvik</i>	71.32°N, 156.62°W	8-20 m
Oliktok Point (Alaska) <i>oliktok</i>	70.50°N 149.89°W	2-6 m
Whitehorse (Canada) <i>whitehorse</i>	60.71°N, 135.07°W	682 m
Eureka (Canada) <i>eureka</i>	80.08°N 86.42°W	0-610 m
Iqaluit (Canada) <i>iqaluit</i>	63.74°N, 68.51°W	5-11 m
Alert (Canada) <i>alert</i>	82.49°N, 62.51°W	8-210 m
Summit (Greenland) <i>summit</i>	72.58°N, 38.48°W	3210-3250 m
Ny-Ålesund (Svalbard) (Zeppelin station) <i>nyalesund</i>	78.92°N, 11.53°E (78.9°N, 11.88°E)	0-30 m (473 m)
Sodankylä (Finland) <i>Sodankylä</i>	67.37°N, 26.63°E	198 m
Pallas (Finland) <i>pallas</i>	67.97°N, 24.12°E	305 m



Tiksi (Russia) <i>tiksi</i>	71.60°N, 128.89°E	1-30 m
Cherskii (Russia) <i>cherskii</i>	68.73°N, 161.38°E (68.51°N, 161.53°E)	8 m (16 m)
Ice Base Cape Baranova (Russia) <i>baranova</i>	79.3°N, 101.7°E	24 m

Arctic Ocean sites

SHEBA location <i>sheba</i>	165°W, 76°N	Sea level
Arctic Ocean 1 (Gakkel Ridge) <i>ao1</i>	10°E, 85°N	Sea level
Arctic Ocean 2 (North Pole) <i>ao2</i>	0°E, 90°N	Sea level
Arctic Ocean 3 (Canada Basin) <i>ao3</i>	135°W, 81°N	Sea level

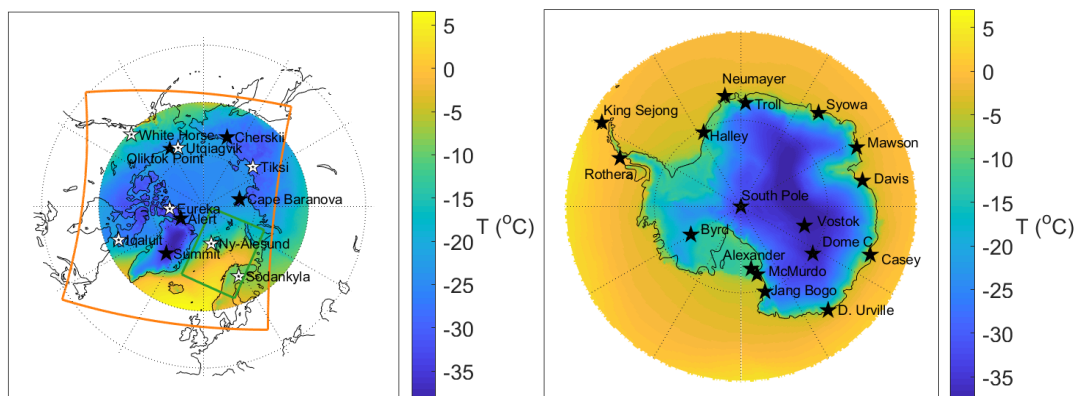
Antarctic land sites

Alexander Tall Tower <i>alexander</i>	79.01°S, 170.72°E	55 m
Casey <i>casey</i>	66.28°S, 110.53°E	30 m
Davis <i>davis</i>	68.58°S, 77.97°E	
Dome C <i>domec</i>	75.08°S, 123.34°E	3233 m
Dumont d'Urville <i>dumont</i>	66.66°S, 140.01°E	0-50 m
Halley IV <i>halley</i>	75.58°S, 26.66° W	130 m
King Sejong (King George Island) <i>kingsejong</i>	62.22°S, 58.79° W	10 m



Georg von Neumayer <i>neumayer</i>	70.65°S, 8.25°W	42 m
Mawson <i>mawson</i>	67.60°S, 62.87°E	15 m
Syowa (Showa) <i>syowa</i>	69.00°S, 39.59°E	18-29 m
Jang Bogo (Terra Nova Bay) <i>jangbogo</i>	74.62°S, 164.23°E	36 m
Amundsen-Scott South Pole <i>southpole</i>	90°S, 0°E	2835 m
Byrd <i>byrd</i>	80.01°S, 119.44°W	1539 m
Rothera <i>rothera</i>	67.57°S, 68.13° W	4 m
Vostok <i>vostok</i>	78.46°S, 106.84°E	3489 m
McMurdo (Scott base) <i>mcmurdo</i>	77.85°S, 166.67°E (77.85°S, 166.76°E)	10 m (10 m)
Troll <i>troll</i>	72.01°S, 2.54°E	1275 m

100 Table 1: List of YOPPSiteMIP observatory locations: name, *name as used in filenames*, latitude, longitude and elevation. Where an elevation range is stated, this is because the instruments at a given observatory extend over a range of values due to variations in local topography.



110 **Figure 1:** Maps of the ERA5 2m-temperature climatology (1990-2019) for February-March (time of NH-SOP1) for Arctic (left) and for November-February (SH-SOP) for Antarctic (right). The observatories used in YOPPsiteMIP are marked with stars. White stars indicate the sites where MODFs are currently available, which are the subject of this study; black stars indicate the sites whose MODFs are not yet complete. The orange and green boxes depict the extent of the ECCC-CAPS and AROME-Arctic domains respectively.

The purpose of this paper is two-fold: firstly, to document the first version of the YOPPsiteMIP dataset along with a basic description of the forecasting systems and their respective MMDFs that are archived at the YOPP Data Portal, hosted by the Norwegian Meteorological Institute (MET Norway). Secondly, the paper presents a multi-site evaluation of seven forecasting systems during NH-SOP1, at seven Arctic observatories that have produced MODFs. The locations are indicated by the white stars in Figure 1a and the MODFs and details of the sites are described in Morris et al., (in prep).

2 Description of simulations, model formulation and output protocol

120 To date, six NWP centres have submitted forecasts from seven forecasting systems for SOP1 & SOP2, with two systems submitted for the SH-SOP (see Table 2). Four of the systems are global:

- The Integrated Forecasting System from the European Centre for Medium-Range Weather Forecasts (ECMWF-IFS; Day et al., 2023),
- The Action de Recherche Petite Echelle Grande Echelle from Meteo France (ARPEGE-MF ; Bazile and Azouz, 2023a),
- 125 • The Semi-Lagrangian, based on the absolute vorticity equation from the Hydrometeorological Research Centre of Russia (SLAV-RHMC, Tolstykh, 2023) and,
- The Icosahedral Nonhydrostatic Model from Deutscher Wetterdienst (DWD-ICON; Frank, 2023).

Three are regional:

- 130 • The Canadian Arctic Prediction System from Environment and Climate Change Canada (ECCC-CAPS; Casati, 2023)
- and two versions of Applications of Research to Operations at Mesoscale (AROME) from Meteo France (AROME-MF; Bazile and Azouz, 2023b) and from MET Norway (AROME-Arctic; Remes, 2023).

The domain boundaries of the regional forecasting systems can be seen in Figure 1 (note that only two of the observatories are within the AROME domain). The forecasts analysed here were initialised at 00 UTC for each day of the SOPs (although 12UTC forecasts are also available on the archive for many of the systems). The forecast leadtime varies between the different systems but all forecasts are at least two days long (see Table 2 and Figs 2 & 3).

The files for some of the systems (CAPS, SLAV, ARPEGE, AROME-MF) are provided with multiple grid-points, centred on the observatory location. For others only a single grid-point was provided. Multiple grid-points centred around the observatory



140 location were requested because many of the observatories are located on coasts and there are issues with grid-points being
over ocean, over land or blended. In this study when there are multiple grid points we choose the closest 100% land point to
the supersite location. The grid resolutions range from 2.5 km to ~30 km and the model timestep varies from 1.5 to 7.5 min
(see Table 2).

145 The models have quite a diverse mixture of formulations for atmospheric dynamics, land surface, sub-grid scale
parameterisations and initialisation/data assimilation procedures. More details about the simulations with specific models are
provided below and a summary of the key model components/parameterisations used in each model is included in Table 3.

2.1 IFS-ECMWF

150 MMDFs for the operational forecasts with the IFS high resolution deterministic forecasts are available for the period starting
Jan 2018. The initial forecasts are produced with IFS cycle 43r3 which was an atmosphere only model with persisted sea ice
and anomaly SSTs. From 5 June 2018 (i.e. before SOP2) the forecasts were produced with cycle 45r1 which included dynamic
sea ice and ocean fields (see Day et al., 2022 for more information). Although the model version changes the horizontal (~9km)
and vertical resolution (L137) are the same in all SOPs. The data archived in the MMDFs is provided at the model timestep
155 (7.5 min) for a single model grid point closest to the observatory. In addition to the grid point data a number of parameters
(including albedo, surface temperature and surface energy fluxes) are provided on the land-surface model tiles to enable
detailed evaluation of processes even at heterogeneous sites. A complete description for the two versions of the IFS can be
found here: <https://www.ecmwf.int/en/publications/ifs-documentation>.

160 2.2 ARPEGE-MF

The version of ARPEGE submitted to YOPPSiteMIP was a pre-operational version based on the cy43t2_op1 operational
system but coupled with the 1D sea-ice model GELATO (Bazile et al. 2020). The resolution of the model used for these
simulations is the same as is used operationally at Meteo France which is variable (using a stretching factor of 2.2) with the
pole (highest resolution of 7.5 km) over France for SOP1 and SOP2 and over Antarctica in SOP-SH and 105 vertical levels.
165 The horizontal resolution is about 8-9 km over the North-Pole and timeseries have been provided for the three SOPs in the
MMDF format for the 21 YOPP observatories with an hourly output for both state variables (instantaneous) and fluxes
(accumulated).

2.3 SLAV-HMRC

170 MMDFs were produced by the SLAV model (Tolstykh et al., 2018) for both SOP1 and SOP2 containing 7-day forecasts
starting at 00 UTC. The output is available for 4 horizontal grid points surrounding selected observatories, every 15 minutes
(i.e. every fourth timestep). Depending on variable, the output is instantaneous or a 15-min averaged value. Data for 13 of the
Arctic observatories in Table 1 are provided. Selection of observatories is based on model resolution in latitude which is
relatively low, ~16 km in Northern polar areas; also, the ao2 point is not included because the model grid does not contain the
175 poles.

2.4 ICON-DWD

MMDFs from DWD's ICON (Zängl et al., 2015) are available from February 2018 to June 2020 containing 7.5-day forecasts
starting at 00 and 12 UTC for Sodankylä, Ny-Ålesund, and Utqiagvik (Barrow). The mesh width is 13 km. Different model
180 versions are used during this period. In February icon-nwp-2.1.02 was used followed by icon-2.3.0-nwp0 during 2018-02-14
to 2018-06-06, and from 2018-09-19 to 2018-12-05 icon-2.3.0-nwp2 was in operation. Since 2018-02-14, a new orographic
data set came in operations, however, for the 3 data points provided the changes were less than 1 m in height. The sea ice



analysis used in ICON, was based on the Real-Time Global SST High Resolution Analysis of NCEP until 2018-07-16. Since then it is based on the Operational Sea Surface Temperature and Sea Ice Analysis (OSTIA; Donlon et al., 2012). To represent variations of subgrid scale surface characteristics ICON uses a tile approach. Since 2018-07-16 the tile values of surface fluxes, and other tile dependent variables are included in the MMDFs in addition to the grid average values. Hourly output is available based on a timestep of 120s.

2.5 CAPS-ECCC

MMDFs for ECCC-CAPS are available for the whole period from February 2018 to December 2018. Prior to the 28th of June 2018 CAPS was uncoupled and run with the GEM version 4.9.2. After the 29th of June 2018 CAPS was coupled with the Regional Ice and Ocean Prediction system (RIOPS) and run with the GEM version 4.9.4. Atmospheric Lateral Boundary Conditions (LBCs) and initial conditions (ICs) are from ECCC Global Deterministic Prediction System (GDPS). Initial surface fields are from the Canadian Land Data Assimilation System (CaLDAS). The CAPS timeseries are produced for a beam of 7 x 7 grid-points centred on each of the twelve land-based Arctic observatories listed in Table 1. Timeseries up to 48 hours leadtime are made available for the daily runs initialized at 00 UTC. The data is archived with a time frequency of 7.5 min, equivalent to five timesteps of 90 s each.

2.6 AROME-ARCTIC

MET Norway utilises the HARMONIE-AROME (HIRLAM–ALADIN Research on Mesoscale Operational NWP in Euromed–Application of Research to Operations at Mesoscale) model configuration (Bengtsson et al., 2017) for operational weather forecasting for the European Arctic with the name AROME-Arctic (Muller et al., 2017). AROME-Arctic MMDFs are based on the operational forecasts (cy40h.1) and are available for the SOP1 and SOP2 at Sodankylä and Ny-Ålesund. LBCs are derived from the ECMWF IFS-HRES described in Section 2.1. Assimilation of conventional and satellite observation with 3DVAR in the upper atmosphere, optimal interpolation of snow depth, screen level temperature and relative humidity in the surface model. Temperature tolerance in the surface assimilation scheme was increased on 15 March 2018 to better assimilate observed low temperatures. The data archived in the MMDFs are provided hourly for the single model grid-point closest to the site. Model data for the full domain in its original format are also available via thredds.met.no.

2.7 AROME-MF

The AROME -MF system from Météo-France and AROME-ARCTIC from MET Norway are both configurations of the same model system but use different parameterizations of turbulence, shallow convection, cloud microphysics and sea ice. The system used for the YOPPsiteMIP differs from the operational AROME-France configuration (Seity et al., 2011) and the version evaluated for SOP1 in Koltzow et al., (2019) in that it is coupled with the GELATO 1D sea ice model. However, the domain (see Figure 1a), horizontal and vertical grid are exactly the same as the AROME-ARCTIC operational system (see Section 2.6). The ICs and LBCs are interpolated from the global model ARPEGE-MF simulation described above (Section 2.2). The MMDF files have been produced for Ny-Ålesund, Sodankylä and Pallas with hourly output.

2.8 Output format

For each forecast initial time and each forecasting system a single netCDF file containing all variables was archived following the MMDF format, which use the same nomenclature, metadata, and structure as the MODFs. In order to be able to assess process representation, the YOPPsiteMIP protocol requested that atmospheric fields were provided on native model vertical levels and all fields should be provided with high frequency (every 5 or 15 minutes), ideally at the frequency of the model timestep if practical.

225



The actual variables archived, frequency and number of grid-points, vary from model to model. For example, ECCC provided a comprehensive set of parameters for the CAPS model focusing on precipitation and clouds microphysics to allow studies on the representation of different types of hydrometeors by the P3 scheme (Morrison and Milbrandt, 2015; Morrison et al., 2015; Milbrandt and Morrison, 2016). A full list of requested variables, along with a schema for producing the MDFs are described in a document known as the H-K Table (Hartten and Khalsa, 2022). The table is available in both human and machine-readable form (PDF and JSON, respectively). The H-K Table relies on standards and conventions commonly used in the earth sciences, including netCDF encoding with CF naming and formatting conventions and is an evolving document that is expected to evolve to fulfil the requirements of future MMDFs and MODFs (Gallagher et al., in prep.). The prescribed metadata make data provenance clear and encourage proper attribution of data origin (see further information in Uttal et al., 2023).

235

Although we only focus on model performance during SOP1, a full set of MMDFs and MODFs was produced for both SOPs. The MODFs for Iqaluit (Huang et al., 2023a), Whitehorse (Huang et al., 2023b), Utqiagvik (formerly known as Barrow: Akish and Morris, 2023a), Eureka (Akish and Morris, 2023b), Tiksi (Akish and Morris, 2023c), Ny-Ålesund (Holt, 2023) and Sodankylä (O’Conner 2023) are described in detail in Morris et al., (2023) along with descriptions of the site geography.

240

MMDFs have also been produced for the SH-SOP with the ECMWF-IFS and ARPEGE models (See Table 2), but no MODFs for the Antarctic observatories have been produced yet.

Centre	Model-name	Global/Regional and horizontal/vertical resolution	Timestep/output frequency/forecast length	Version	Key Reference(s)	SOPs in YOPP portal
ECMWF	IFS	Global: 9km/L137	7.5min/7.5min/3d	Cy43r3 for SOP1, Cy45r1 for SOP2 & SOP-SH	Buizza et al., (2017)	SOP1, SOP2 & SOP-SH
Meteo-France	ARPEGE-GELATO	Global: 7.5-25km/L105	240s/60min/4d	cy43t2_op2	Pailleux et al. (2014)	SOP1, SOP2 & SOP-SH
Meteo-France	AROME-Arctic	Regional: 2.5km/L65	50s/60min/2d	cy43t2_op2	Seity et al., (2011)	SOP1 & SOP2
ECCC	CAPS	Regional: 3km/L62	1.5min/7.5min/2d	vn1.0.0 for SOP1 & vn1.1.0 for SOP2	Milbrandt et al., (2016) Casati, et al., (2023)	SOP1 & SOP2



DWD	ICON	Global: ~13km/L90	2min/60min/7.5 d	icon-nwp-2.1.02, icon-2.20-nwp0, icon-2.30-nwp0, icon-2.30.nwp2	Zängl et al., (2015) Prill et al., (2020)	SOP1 & SOP2
HMCN	SLAV	Global: ~20km/L51	3.75min/15min/ 3d	SLAV20 (2018)	Tolstykh et al., (2018) Tolstykh et al., (2017)	SOP1 & SOP2
MET Norway	AROME- Arctic	Regional: 2.5km/L65	50s/60/2d	HARMONIE- AROME cy40h	Müller et al. (2017) Bengtsson et al., (2017)	SOP1 & SOP2

245 **Table 2. Summary of forecasting systems**



Model-name	Land-surface model	Surface layer/fluxes	Turbulent diffusion	Orographic drag	Convection	Cloud microphysics	Radiation	Dynamical core
IFS	HTESSEL: Balsamo et al., (2009)	K-diffusion with stability functions of Dyer (1974) and Höglström (1988) and Holtslag and De Bruin (1988) in unstable conditions and for stable conditions	EDMF Köhler et al., (2011) in unstable conditions and K-diffusion (Louis, 1979; Sandu et al., 2013) in stable conditions	Following Lott and Miller (1997) and Baines and Palmer (1990)	mass-flux for deep, shallow and mid-level convection: Tiedtke (1993) and Bechtold et al. (2008)	double moment scheme with four categories of hydrometeor Forbes and Ahlgren (2014)	EcRad (Hogan and Bozzo, 2018) Is based on the Rapid Radiation Transfer Model (RRTM, Mlawer et al., 1997; Iacono et al., 2008)	Spectral/FE/H
ARPEGE	SURFEX: Masson et al., (2013)	K-diffusion with modified version of Louis (1979)	TKE: Cuxart et al., (2000) with a modified mixing length (Bézile et al. 2011)	Scheme described in Catri et al., (2008) following Lott and Miller (1997) for mass flux for shallow gravity wave drag, and an envelope orography approach (after Wallace et al., 1983)	Mass flux for deep convection following Bougeault (1985) and mass flux for shallow convection following Bechtold et al., (2001)	Single moment with five categories of hydrometeor (Sietty et al., 2012)	RRTM	Spectral/FE/H
AROME-MF	SURFEX: Masson et al., (2013)	K-diffusion with stability function of Louis (1979)	TKE: Cuxart et al., (2000)	N/A	Deep convection is explicitly represented and shallow uses the Pergaud et al. (2009) EDMF scheme.	Single moment with six categories of hydrometeor (ICE3; Pinty and Jabouille 1998)	RRTM	Spectral/FD/NH
CAPS	ISBA: Noilhan and Planton (1989) and Bélair et al. (2003)	K-diffusion with stability functions of Delage and Girard (1992) in unstable conditions and Delage (1997) in stable conditions.	TKE with statistical representation of subgrid-scale cloudiness (Mois-TKE: Bélair et al. (2005))	Lott and Miller (1997)	Deep convection from the Kain and Fritsch (1990) mass flux scheme and shallow convection from a Kuo-transient scheme (Bélair et al., 2005)	Double moment with Predicted Particle Properties (P3; Morrison and Milbrandt, 2015; Morrison and Milbrandt and Morrison, 2016)	Correlated-k radiative transfer scheme (Li and Barker, 2005)	Gridpoint/FE (horizontal)&FD(vertical)/NH (Coté et al., 1998a,b; Girard et al., 2014)



3 Evaluation of basic surface meteorology and vertical profiles

3.1 Evaluation/Scores

- 250 As mentioned in the introduction, the combination of MODFs and MMDFs allow detailed process-oriented diagnostics to be performed for the models. However, it is first important to assess what the errors are for standard variables such as 10m wind speed and 2m temperature. This first step is important because if they are stationary with leadtime one can simply consider a 24hr time range in the forecasts such as T+25 until T+48 (the second day of the forecast), simplifying the analysis.
- 255 The 2m temperature errors have quite different properties at each site and for each model (Fig 2). The models are typically too warm at Utqiagvik and Tiksi and too cold at Ny-Ålesund and Whitehorse, with the sign of the bias varying between the models at Iqaluit and Eureka. At both Sodankylä and Whitehorse, which are situated at lower latitudes than the other sites, there is a distinct diurnal cycle in the bias and standard deviation that is not there at higher latitude sites. At both sites the night-time temperature bias is typically more positive than the daytime bias, indicating an underestimate of the diurnal temperature range.
- 260 In the case of the CAPS and the IFS, the bias in the diurnal cycle at these observatories are representative of those seen over wider region (e.g. Casati et al., 2023 and Haiden et al., 2018).

In terms of wind speed, the forecasts all have a positive wind speed bias at Utqiagvik and a negative bias at Iqaluit and Whitehorse (Fig 3). At Tiksi, Eureka, Sodankylä and Ny-Ålesund, the sign of the bias varies between the models. Interestingly, the largest inter-model spread and biases in wind speed is observed at the sites with the most complex orography (i.e. Iqaluit, Ny-Ålesund, Eureka and Tiksi: see Fig 2 of Morris et al., 2023), likely due to the difficulties in representing the mesoscale flow patterns typically generated in such locations. Interestingly, there does not seem to be an obvious benefit from the increased resolution, with the AROME configurations and CAPS model actually having worse biases than the lower resolution global models at Ny-Ålesund.

270 Although there is some sub-daily variability with a diurnal frequency in the bias, more pronounced in wind speed bias (Figs. 2 and 3), the size of the biases does not grow dramatically with time. Thus, we consider a 24hr time range between the T+25 and T+48 forecast steps (i.e. the second day of the forecast) to be representative of the general error, simplifying the analysis.

275

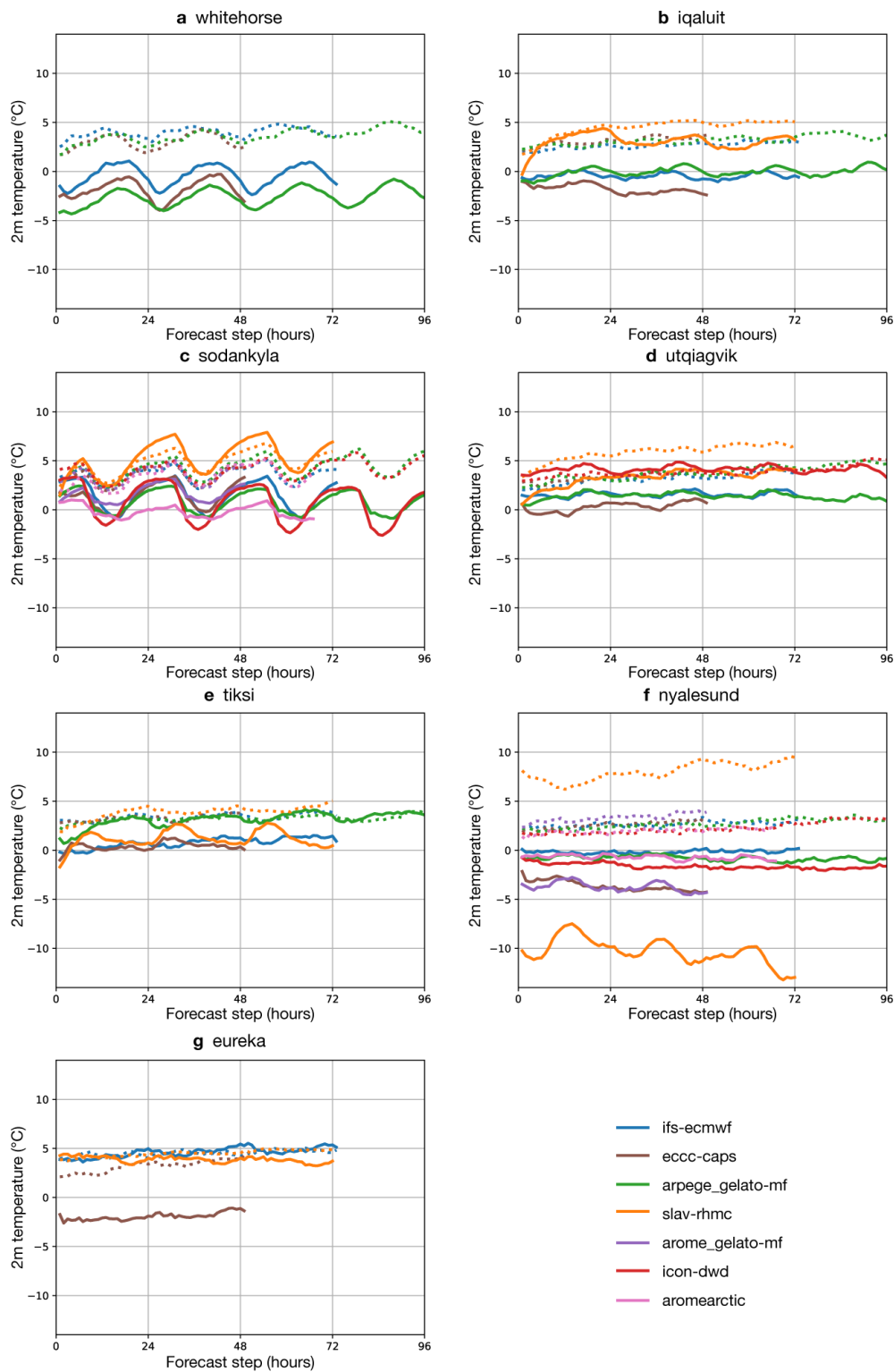
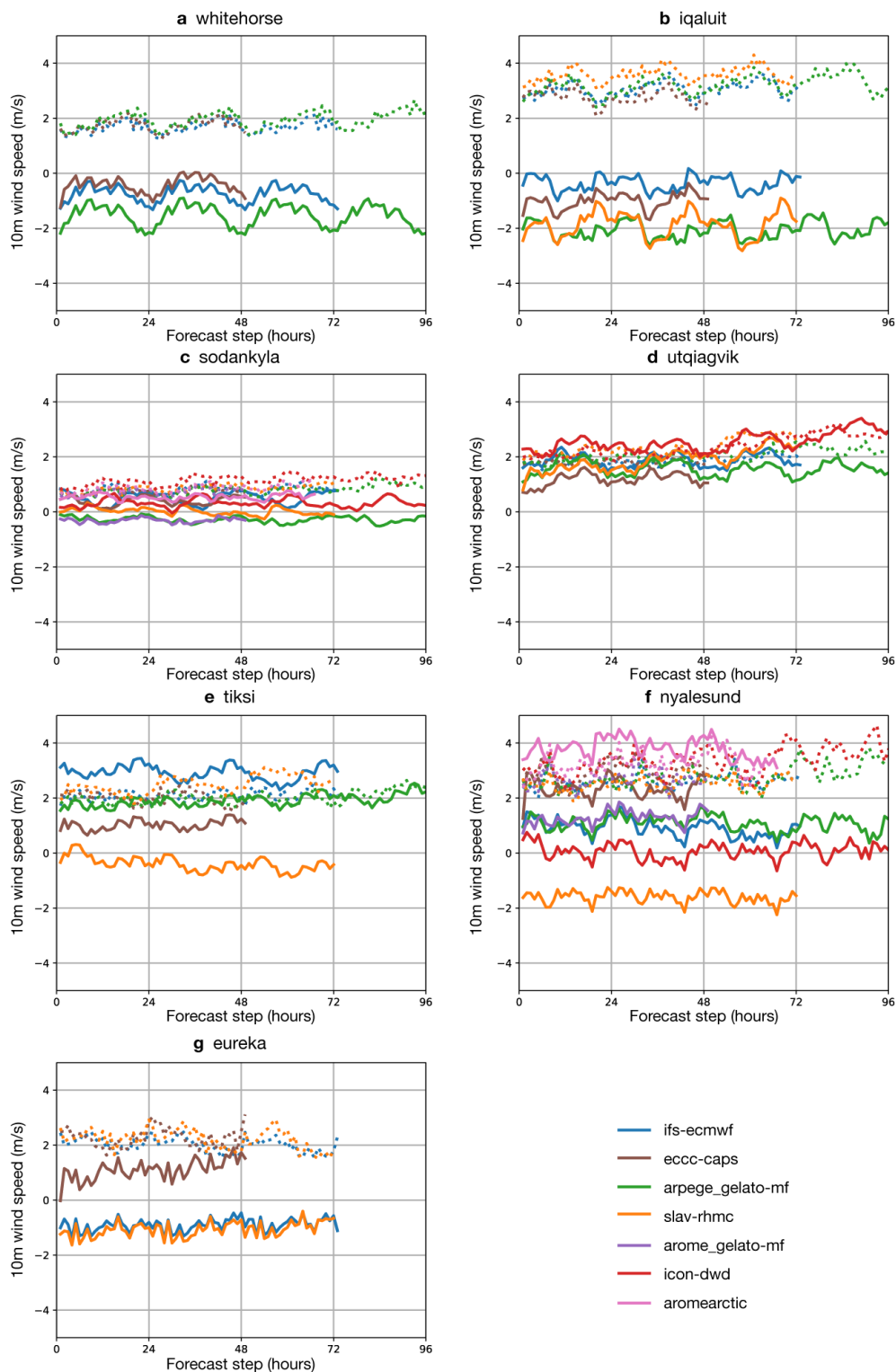


Figure 2: Mean bias (solid lines) and standard deviation (dashed lines) of the 2m temperature error (in °C) at each observatory (see Figure 1a) for forecasts initialised at 00z during SOP1, described in Table 2.



280

Figure 3: Mean bias (solid lines) and standard deviation (dashed lines) of the 10m wind speed error (in m s^{-1}) at each observatory for forecasts initialised at 00z during SOP1.



3.2 Vertical profiles

285 To gain further insights we investigate the vertical structure of the errors by comparing the model output to observations from
radiosonde and tower. The median temperature and specific humidity within the boundary layer is overestimated at Tiksi,
Eureka, Utqiaġvik and Iqaluit (see Fig 4) and the models underestimate the strength of temperature and humidity inversions
as a result. The picture is more mixed at Ny-Alesund and Sodankylä where all models are too cold, and two out of the three
models are too dry at Whitehorse.

290

The biases in the upper air temperatures, 2m air temperature, and the surface skin temperature tend to go hand-in-hand with
each other, i.e. model with warmest/coldest surface temperature tends to have the warmest/coldest 2m and upper air
temperatures. As a result, the mean 2m temperature errors seen in Fig 2 give a sense of the sign of the error in the lowest 100m,
or so, of the atmosphere. This coupling between the lowest model level, the surface skin temperature and the 2m-temperature
295 is to be expected, since the 2m-temperature is a diagnostic calculated as a function of the lowest atmospheric model layer and
the surface skin temperature.

Air temperature variability in the lower boundary layer is generally underestimated by the models, except at Iqaluit (Fig 5).
This generally translates to an underestimation of the 2m temperature variability at these sites. Interestingly, at Ny-Alesund
300 some models severely overestimate the 2m temperature variance despite underestimating the variance aloft. For specific
humidity the observed inter-quartile-range tends to sit within the range of the models, however it is over-estimated at Eureka
and underestimated at Tiksi and Whitehorse in the lower boundary layer.

The median of the modelled wind speed is too high in the boundary layer at Sodankylä, Utqiaġvik and Tiksi, but more mixed
305 at other sites (Fig 4 & 5). The variance of the wind speed is within the model range, with the exception of Iqaluit, where it is
underestimated. The overestimation of the wind speed at these sites is likely a contributing factor in the underestimation of the
temperature and humidity inversions, since a positive bias in the wind speed will drive excessive turbulent mixing of heat and
moisture inhibiting the decoupling of near-surface and upper air temperatures that occurs during periods of radiative surface
cooling and low wind (Van de Weil et al., 2017). Other factors which could play a role are the radiative forcing at the surface
310 or the response of the surface to radiative forcing. Both aspects will be addressed in the following subsection.

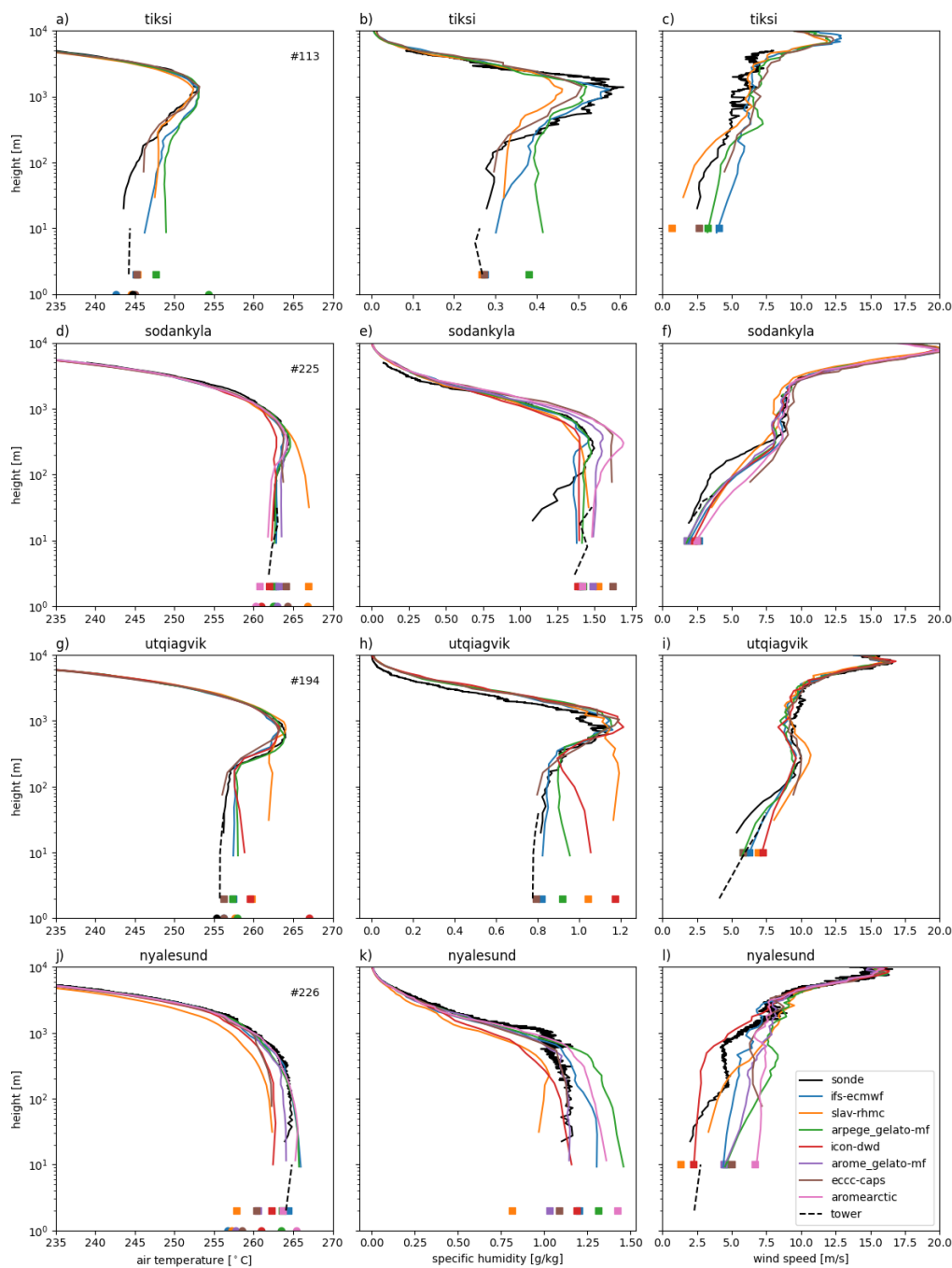


Figure 4: Median temperature (left), specific humidity (middle) and wind speed (right) from the radiosonde (black solid line), the tower (black dashed line), and the numerical models (during the second day of the forecast: colour lines). The mean surface skin temperature is indicated by a dot, 2m temperature (left), 2m specific humidity (middle) and 10m wind speed (right) are shown with a square. Note that wind speed and humidity profiles from the tower are not available in the Tiksi and Ny-Ålesund MODFs respectively. The numbers in the left hand panels correspond to the verification sample size, which was dictated by the availability of radiosonde profiles.

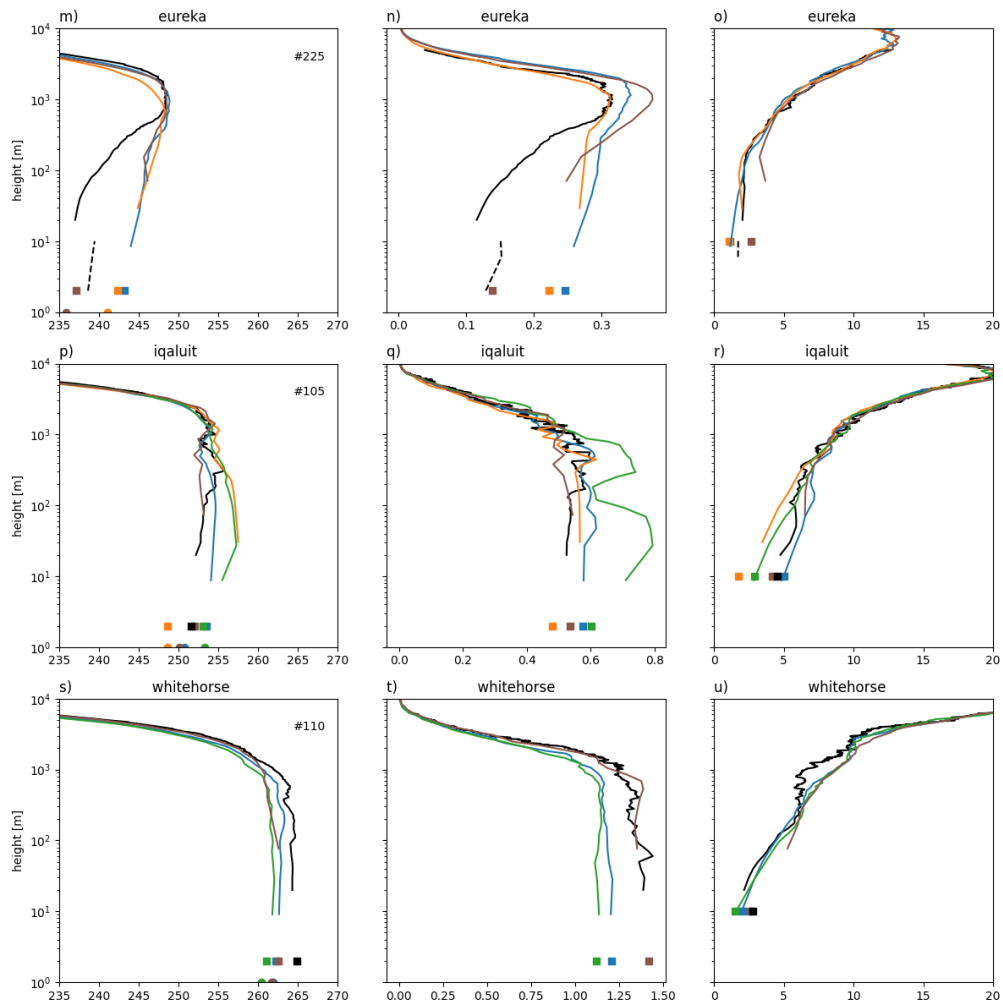


Fig 4 continued.

320

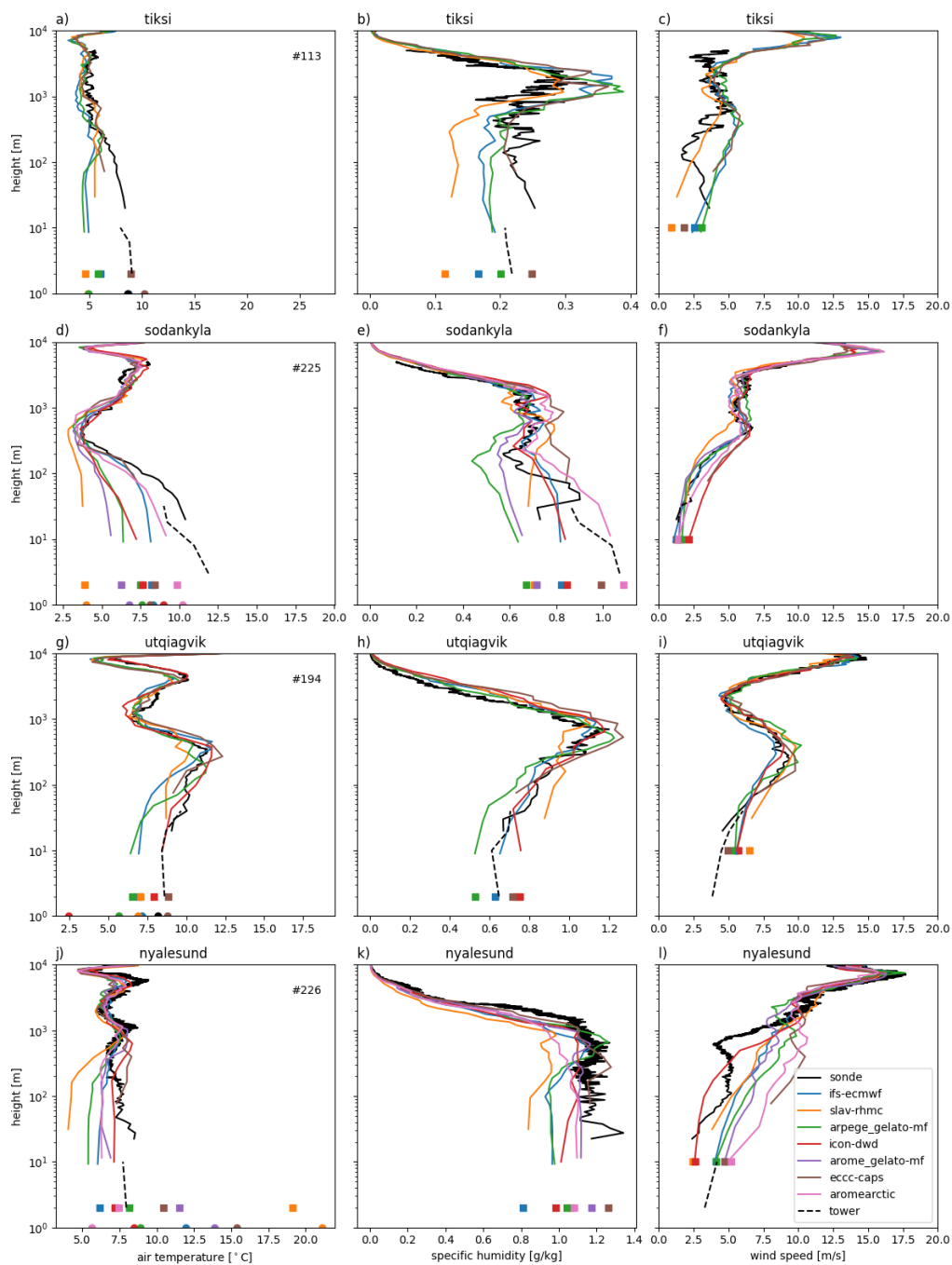
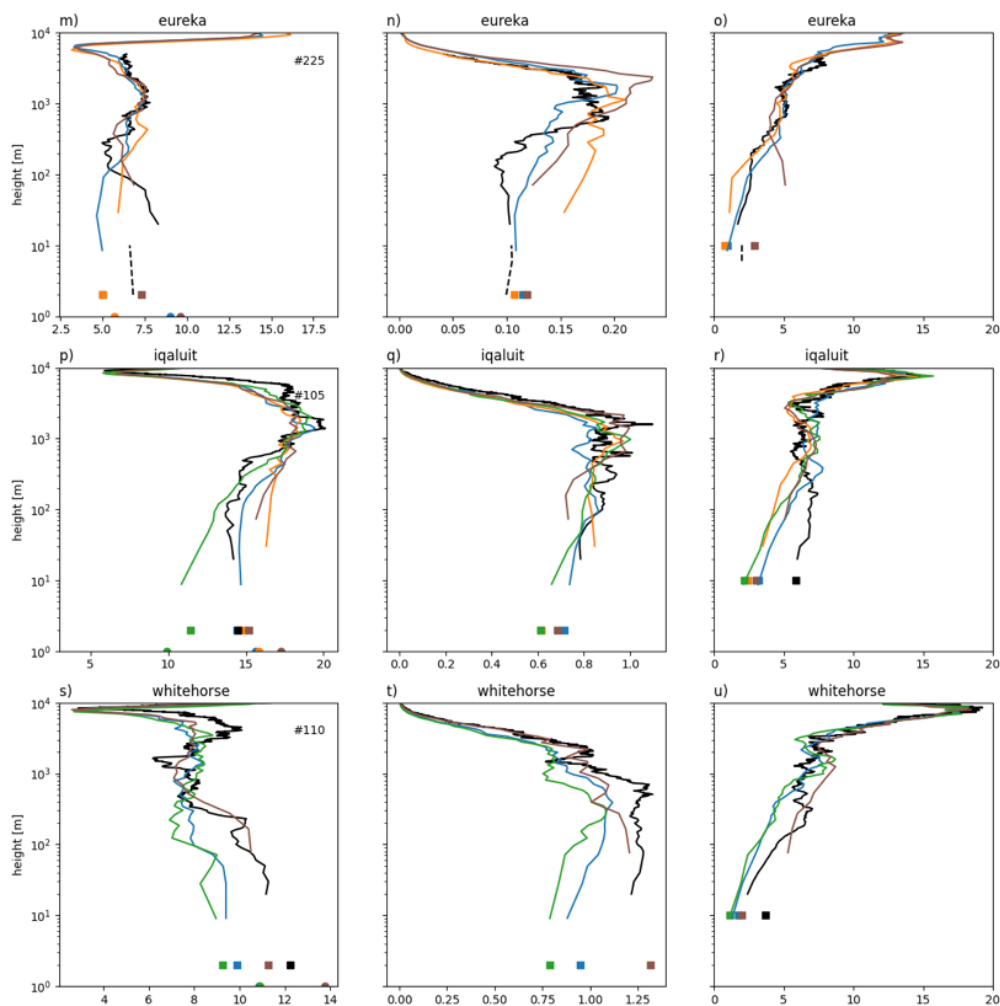


Figure 5: As Figure 4 but showing the Inter Quartile Range.



325

Fig 5 continued.

3.3 Links between errors in boundary-layer temperature variance and surface radiation.

In this section we investigate the role of radiative forcing in the underestimation of near-surface and boundary-layer temperature variability at Sodankylä, Utqiagvik and Tiksi where the models underestimate the temperature variability. At these sites all upwelling and downwelling radiation components are available in the SOP1 MODFs allowing us to investigate whether the suppressed temperature variability is related to suppressed variability in the radiative forcing at the surface, a lack of sensitivity of the near-surface temperature to radiative forcing or something else.

The box plots shown in Fig 6a-c confirm the underestimate of near-surface-temperature Inter-Quartile Range (IQR) at Tiksi (except CAPS), Sodankylä, and Utqiagvik, and further show that the cold tail of the distribution is generally shorter in the models meaning there is a warm bias during cold periods. The warm bias in cold conditions is well known at Sodankylä and is typical of NWP systems (see Atlaskin and Vihma, 2012 and Day et al., 2020), but this feature has not been shown before at the other two sites to our knowledge.

340

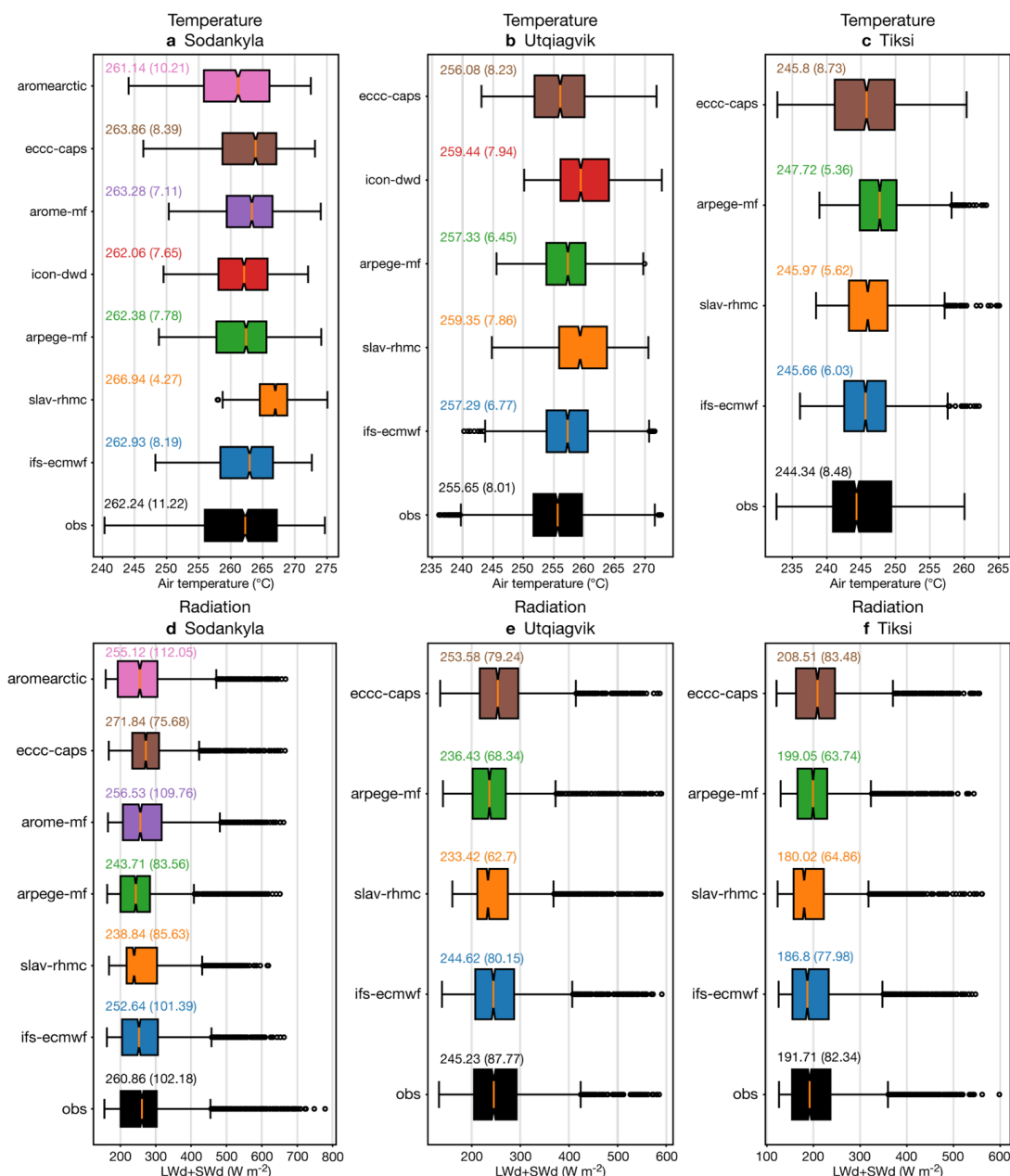


The models typically also show differences in the distribution of the downwelling radiation at the surface, $LW \downarrow + SW \downarrow$ compared to observations (Fig 6d-f). The IQR is underestimated at Tiksi (except for CAPS) and Utqiagvik. However, at Sodankylä all the models overestimate the IQR but also do not capture the highest values of incident radiation observed at the top of the distribution. In this study we will not investigate the causes of these discrepancies between the observed and forecast radiation distributions further, leaving this for a more focussed future study, and will instead move on to focus on the response of the near-surface air temperature and the surface energy budget.

350

355

360



365 **Fig 6.** Boxplots of T2m (a-c) and LW↓+SW↓ (d-f) for Sodankylä, Utqiagvik and Tiksi in observations and during the second day of the forecast. The text above the boxplots states the median (and inter-quartile-range) of each distribution, which are also shown by the orange line and box edges respectively. The 5-95% range is plotted by the whiskers and points outside this are shown in dots.

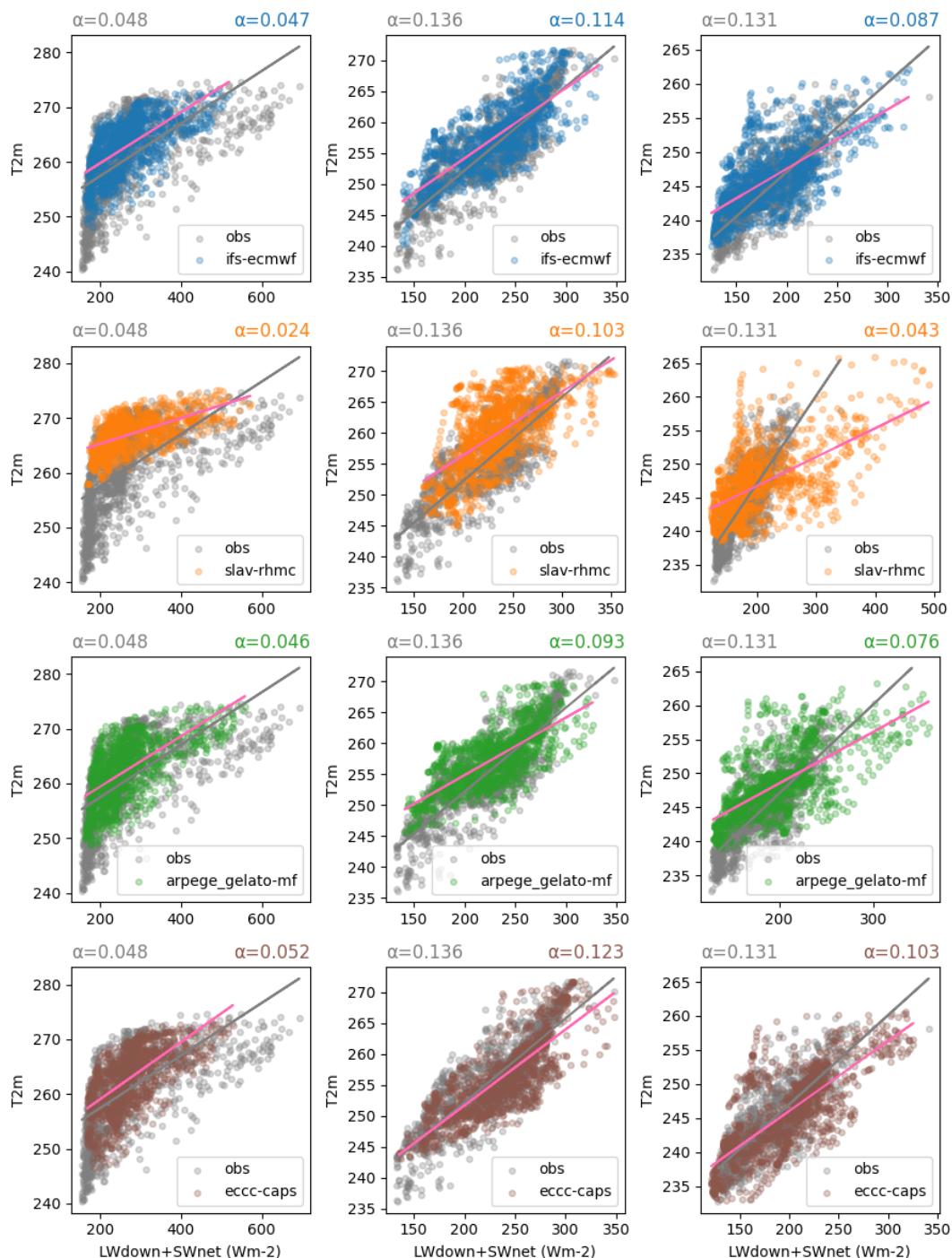
370 As $LW\downarrow + SW_{net}$ is a major driver of 2 m air temperature, errors in 2 m air temperature are either due to errors in this driving term itself, the relationship between $LW\downarrow + SW_{net}$ and 2 m temperature, or a more likely combination of both (assuming that errors in advection are negligible). So looking at how the 2m temperature varies as a function of $LW\downarrow + SW_{net}$ can provide additional information on the causes of error.



375 At Sodankylä, Tiksi and Utqiagvik all the models have a conditional warm 2m temperature bias at low levels of incoming radiation ($LW_{\downarrow} + SW_{net}$) (see Fig 7). At Tiksi, Utqiagvik and Sodankylä the overall sensitivity of T2m to radiative forcing, as measured by the slope of the regression coefficient between 2m-temperature and $LW_{\downarrow} + SW_{net}$ is underestimated in all the models with one exception. The AROME-Arctic model is actually too sensitive at Sodankylä, but captures the observed temperature range at low levels of $LW_{\downarrow} + SW_{net}$.

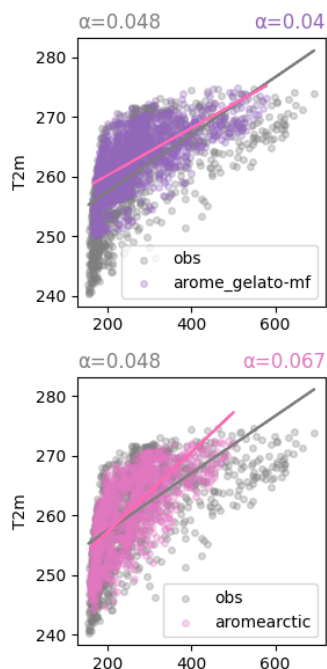
380

Note that the LW components used for Sodankylä in this study, are not those provided in the SOP1 MODF, which are collected at the top of the 45m tower, rather they are from a dedicated radiation tower located near the sounding station where the downwelling component is at a height of 16m and the outgoing is at 2m. These were swapped due to a concern over the accuracy of the LW radiation data collected at the met tower (Roberta Pirazzini, personal communication).



385

Fig 7: Scatter plots of 2m temperature as a function of $LW_{\downarrow} + SW_{net}$ for Sodankylä, Utqiagvik and Tiksi (from left to right). The regression slope between the 2m temperature and the $LW_{\downarrow} + SW_{net}$ is stated in the title, for the observations (in grey) and each model (various colours) during the second day of the forecast.



390

Fig 7 cont.

3.4 Surface energy budget sensitivity to radiative forcing

Further insight can be gained by constructing surface energy budget sensitivity diagrams, following Miller et al. (2018) and Day et al. (2020). The idea here is that the surface energy budget can be separated into a “driving term” ($LW_{\downarrow} + SW_{net}$) and “response terms” (SHF , LHF , GHF , and LW_{\uparrow}). The relationship between the driving term and each response term can be summarised with regression coefficients, e.g. for the SHF :

$$SHF = \alpha_{SHF}(LW_{\downarrow} + SW_{net}) + \beta_{SHF} \quad (1)$$

where each of the α 's can be interpreted as a coupling strength parameter between the driving term and each response term.

These α 's provide direct information on the proportional response of each flux term, expressed as a fraction of the total change in radiative forcing. From this one can see that if, for example, the coupling to the ground heat flux and turbulent fluxes is too strong in the model (i.e. $|\alpha_{GHF_{mod}} + \alpha_{SHF_{mod}} + \alpha_{LHF_{mod}}| > |\alpha_{GHF_{obs}} + \alpha_{SHF_{obs}} + \alpha_{LHF_{obs}}|$) then $|\alpha_{LW_{\uparrow}}|$ will be too small, i.e. surface temperature response will be too weak and vice versa. Similarly, compensating errors in the strength of the coupling to the turbulent fluxes ($\alpha_{SHF_{mod}} + \alpha_{LHF_{mod}}$) and ground heat flux ($\alpha_{GHF_{mod}}$) could result in the right surface-temperature sensitivity, $\alpha_{LW_{\uparrow}}$, but for the wrong reasons. As a result, by comparing the observed and modelled regression coefficients one can derive physical understanding of the causes of model error.

It is clear from Figures 8, 9 and 10 that all the models generally underestimate the surface temperature sensitivity to radiative forcing at Sodankylä, Utqiagvik and Tiksi, because the rate of change in LW_{\uparrow} with changes in radiative forcing, $LW_{\downarrow} + SW_{net}$, i.e. $\alpha_{LW_{\uparrow}}$ is typically too low (i.e. $\alpha_{LW_{\uparrow_{mod}}} < \alpha_{LW_{\uparrow_{obs}}}$). Since the 2m temperature diagnostic in the models is calculated as a function of the surface skin temperature, the underestimation of the sensitivity parameter (the regression coefficient) for 2m-temperature and LW_{\uparrow} and the inability of the models to capture the lowest values of these variables are closely (i.e. comparing Fig 7 to Figs 8, 9 and 10. For example, at Sodankylä the CAPS model T2m and upwelling longwave (LW_{\uparrow}) sensitivities are



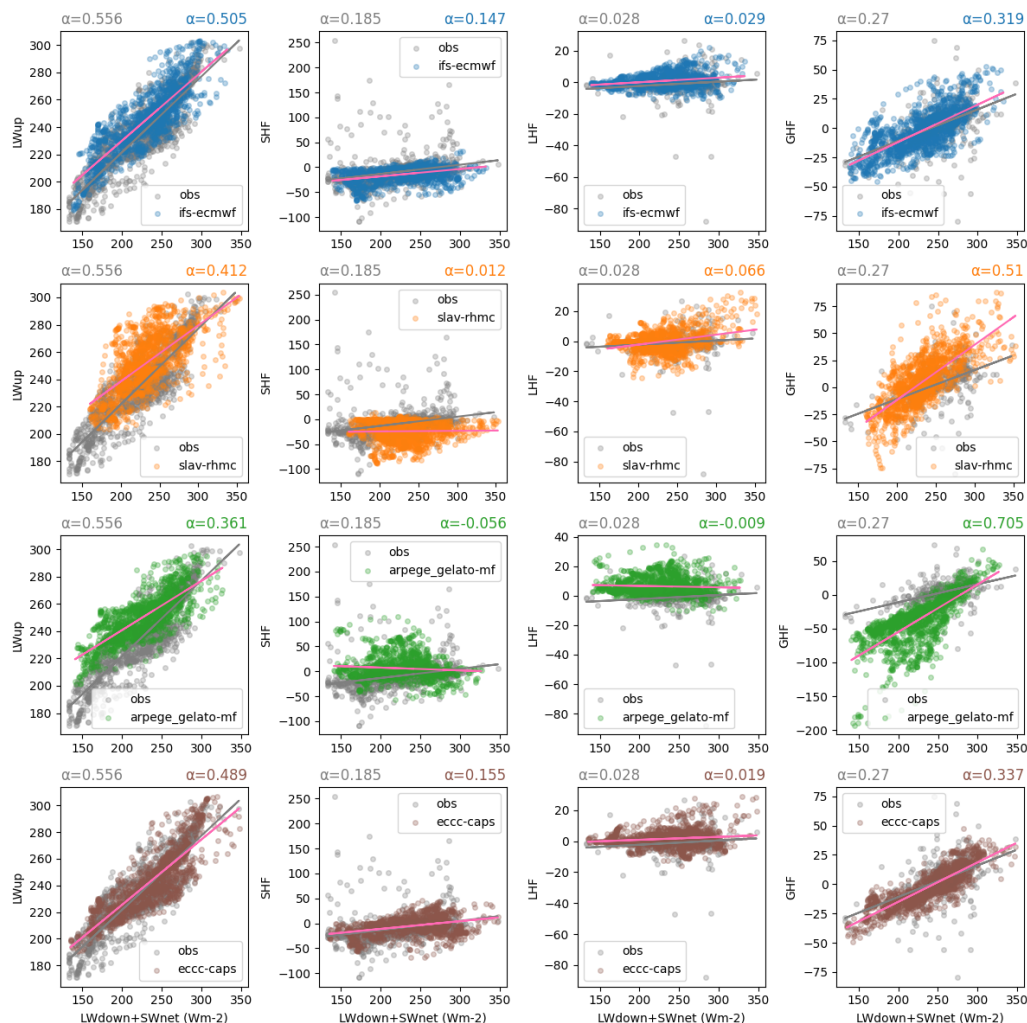
very close to what is observed, AROME-Arctic slightly overestimates these sensitivities and SLAV underestimates them. A
415 similar proportionality can be seen between these properties of the models at the other two sites. Note that because the $LW\uparrow$ at
Sodankylä was observed at 2m and so has rather a small footprint compared to the sensor on the 16m mast, the sensitivity is
more representative of the bare snow than the forest canopy. As a result, one might expect the area mean $LW\uparrow$ sensitivity to
be higher than the value presented here.

420 This mismatch in terms of $LW\uparrow$ sensitivity goes hand in hand with differences in the other α coefficients and by comparing
the sensitivities of the other response terms in the surface energy budget we can develop some hypotheses about what it leading
to this mismatch in surface temperature sensitivities. For example, at Utqiagvik, all the models tend to overestimate the
sensitivity of the GHF , α_{GHF} , which was calculated as the residual of the observed radiative and turbulent fluxes. This can be
an indication of an indication of non-sufficient thermal representation of the land surface, for example lack of a multi-layer
425 snow model (e.g. Day et al., 2020; Arduini et al., 2019). Unfortunately, we are not able to perform a similar calculation as
performed for Sodankylä, to estimate the GHF , as the longwave observations thought to be most reliable, are not co-located
with the other flux observations, or Tiksi, since we don't have the turbulent fluxes in the MODF. As a result, we cannot
calculate the GHF as a residual of the other terms.

430 Where we have turbulent flux observations, we can also evaluate the α_{SHF} and α_{LHF} terms. At Utqiagvik, an underestimation
of the sensitivity of the turbulent fluxes, too low α_{SHF} and α_{LHF} in the ARPEGE and SLAV models goes hand in hand with an
overestimation of α_{GHF} mentioned above. In the IFS and ECCO models are closer to observations with smaller values of α_{GHF}
and larger values of α_{SHF} and α_{LHF} . At Sodankylä, the α_{SHF} varies quite a bit from model to model but all the models where
the LHF was available overestimate the α_{LHF} .

435
At all three sites the relative size of the coefficients varies between the sites, with $\alpha_{LW\uparrow}$, α_{SHF} , α_{GHF} typically being an order
of magnitude larger than α_{LHF} . This is likely to be typical of cold dry snow-covered environments where the magnitude of the
latent heat flux is low. However, the difference in the relative size of the other three terms varies quite a bit between sites with,
for example, the turbulent flux playing a larger role at Sodankylä than at Tiksi and Utqiagvik at this time of year. This reflects
440 the larger surface roughness at Sodankylä associated with the trees at this site.

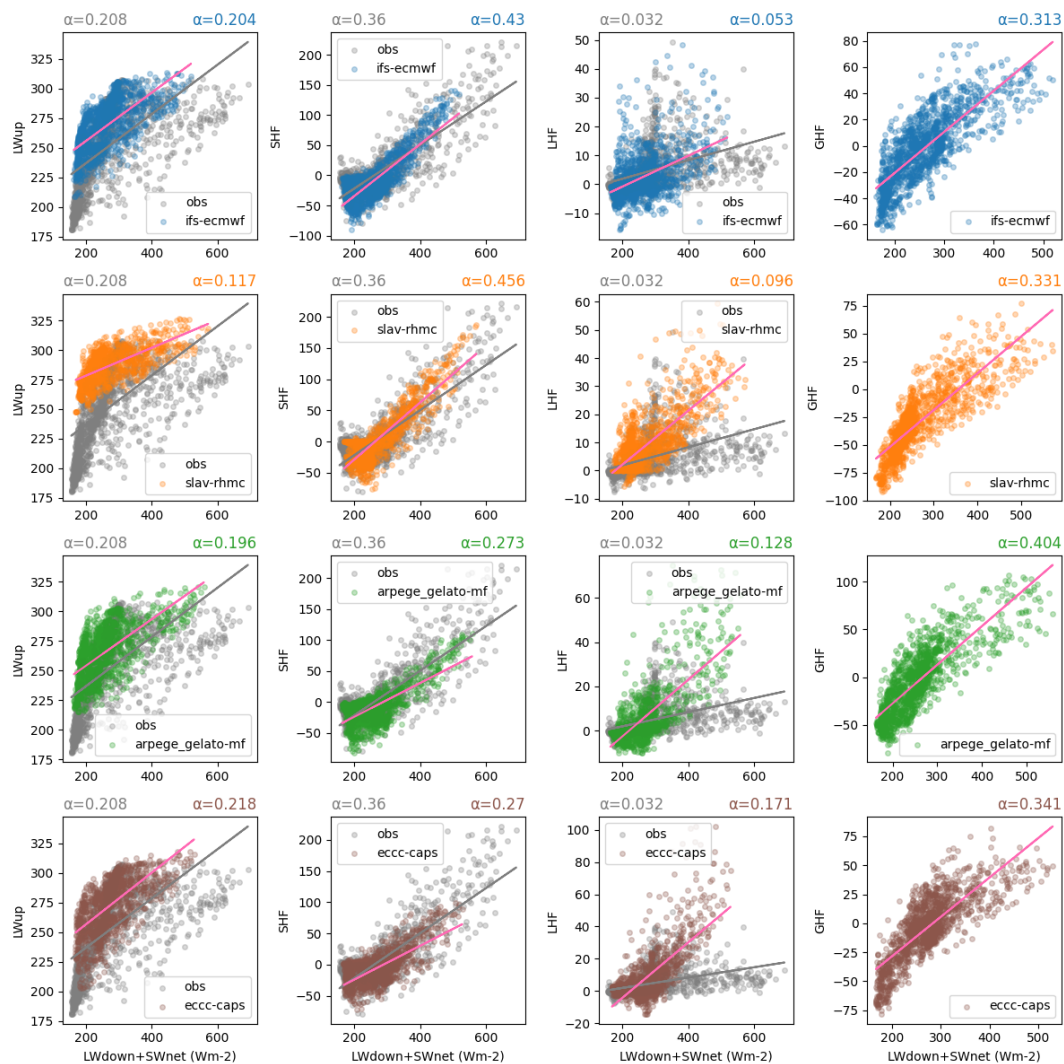
Before moving on it is worth noting that as well as being used to develop hypotheses about the causes of errors related to the
surface energy budget, these process diagrams and sensitivity metrics could also be applied to test new configurations of NWP
systems with modifications to the land-surface, boundary layer or related schemes and evaluate whether such modifications
445 are improving the dynamic behaviour with respect to the surface energy budget in line with observed behaviour or not.



450

Figure 8: Process relationship diagrams and sensitivity parameters for upwelling longwave radiation (LWup; left), sensible heat flux (SHF; middle left), latent heat flux (LHF; middle right) and ground heat flux (GHF; right) at Utqiagvik. Observed values are shown in grey, model values during the second day of the forecast are shown in colour. The line of best linear fit is shown for observations (gray line) and each model (pink line). The sensitivity parameters, α , describing the coupling strength between the driving ($LW_{\downarrow} + SW_{net}$) and each response term are printed above each diagram, with observational (modelled) relationship on the left (right).

455



460 Figure 9: Same as Figure 8 but for Sodankylä.

465

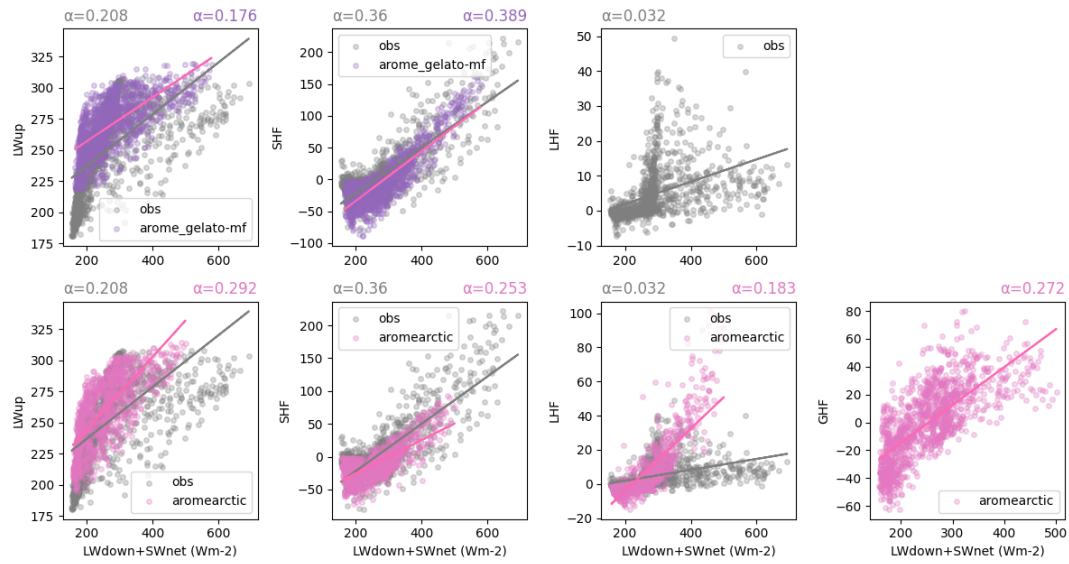
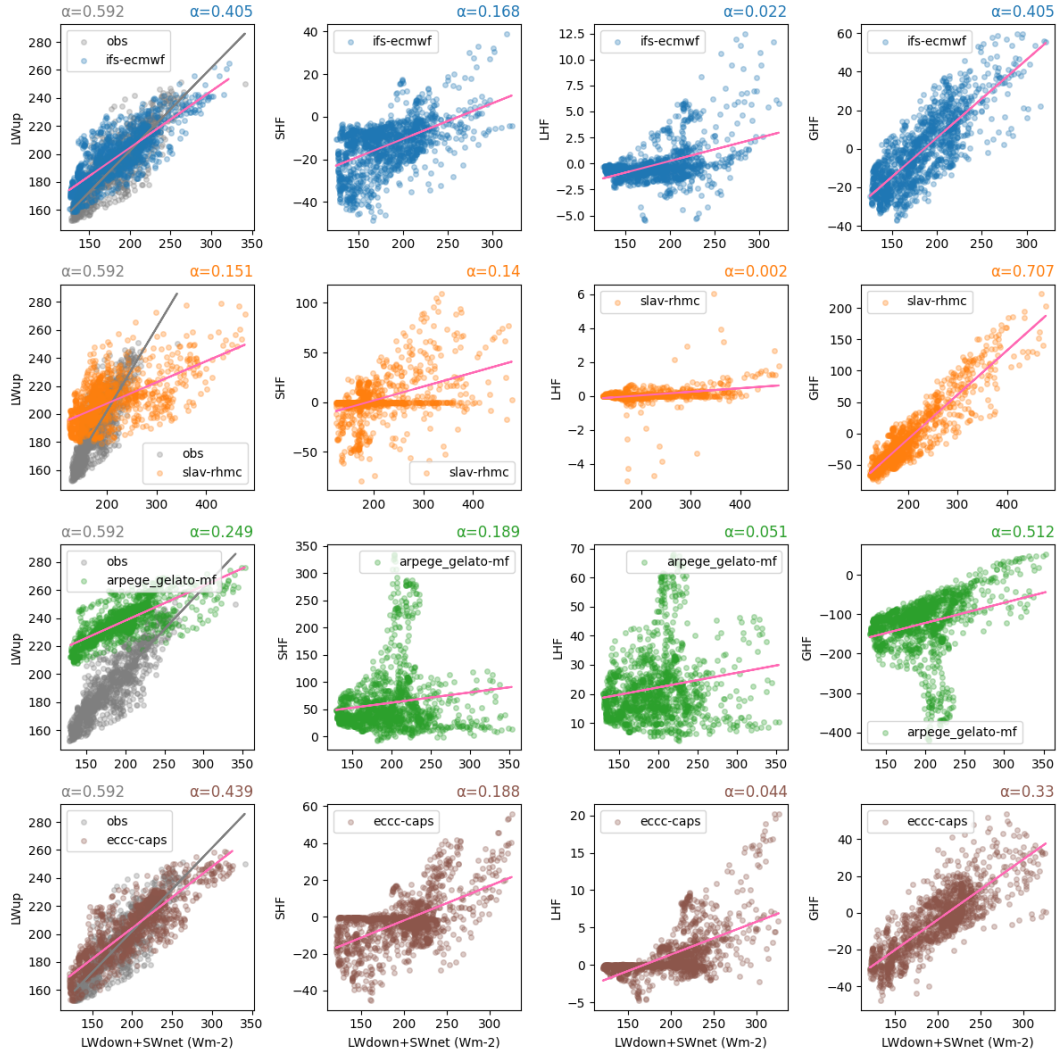


Figure 9: cont.



470 **Figure 10:** Same as Figure 8 but for Tiksi.

3.5 Evapuation of wind stress and sensible heat flux

The previous examples highlight discrepancies between forecast and observations and provide hints as to which processes are responsible for the documented errors. The observed conditions also provide multi-variate targets for updated forecasting systems. However, the observations can also help us evaluate a specific process and thereby target a specific parameter or parameterization to change.

The Sodankylä and Utqiagvik MODFs include turbulent fluxes and profiles of wind speed and temperature allowing us to investigate the parameterisation of turbulent exchanges of heat and momentum at the surface. Turbulent surface fluxes in NWP models are often parameterised according to Monin-Obukhov (M-O) similarity theory where they are related to the gradient in the lowest atmosphere (e.g. Beljaars and Holtslag, 1991):

$$\tau = \rho C_M U_{ref}^2 \quad (2)$$

$$SHF = \rho C_H U_{ref} (\theta_{ref} - \theta_{sfc}) \quad (3)$$



where τ is the wind stress, U is the wind speed, θ is potential temperature, ρ is the air density and the transfer coefficients, C_M and C_H , used in each computation, are a function of the roughness length of momentum and heat, z_{0M} and z_{0H} , and a stability parameter. In these equation the U_{ref} and θ_{ref} are the wind speed and potential temperature at a reference height, which in the case of the models is the lowest atmospheric model level, the height of which varies from around 10 to 30m above the surface depending on the model (see Table 3).

485
490 Successfully parameterizing τ and SHF relies on defining a reasonable function for C_M and C_H and selecting the appropriate parameters and a proper aggregation of the fluxes in the cases of a tiled surface. Because we have observed and forecast values for both the fluxes and the bulk parameters in equations 2 and 3 we can diagnose how appropriate the choices in each model are for the conditions at a particular site. This is done by examining the relationship between the bulk parameters, U and θ , and the fluxes τ and SHF (see Figures 11 to 14), as done previously by Tjernström et al. (2005) and more recently by Day et al. (2020).
495

In the case of wind stress, in neutral conditions, the points in Figures 11 and 12 would sit on the straight line following:

$$\tau = \rho \frac{k^2 U^2}{\left[\ln\left(\frac{z_{ref}}{z_{0M}}\right) \right]^2},$$

500 where z_{ref} is the height of the lowest model level, k is the von Karman constant and z_{0m} is the aerodynamic roughness length. The slope of this line is determined by z_{0m} . However, this formula provides an overly simplified view as the atmospheric stability varies from neutral conditions and as a result there is scatter in the values of τ for any given wind speed.

The relationship between τ and U for Sodankylä (Figure 11) differs between the models and between the models and the observations. An estimate of the observed roughness length was also calculated, following the equation above, after selecting for neutral conditions, and the value is presented in Table 4 along with the value used in each of the models. In the AROME-Arctic and ICON models, τ increases too slowly with increasing U . This is consistent with the fact that the roughness length for momentum is too low in these models, which have roughness lengths an order of magnitude lower than that derived from observations (see Table 4). Increasing z_{0m} in the AROME-Arctic and ICON models would likely reduce the positive bias in
510 the wind median wind speed profile seen in Figure 4. Interestingly, all models fail to adequately capture the spread of τ for a given value of U , likely because the models underestimate the atmospheric stability as is suggested by the weaker than observed thermal stratification indicated by in Figs 4d and 5d. A more detailed study including numerical experimentation would be needed to demonstrate this further.

515 At Utqiagvik, the aerodynamic roughness length is three orders of magnitude lower than at Sodankylä, reflecting the difference in surface type: snow covered tundra compared to the forested taiga of northern Finland (Table 4). Here the IFS and SLAV models have roughness lengths close to those derived from observations, whereas the ARPEGE and ICON have values that are higher. As a result, for a given wind speed the surface stress is too high in these two models (Figure 12).

520

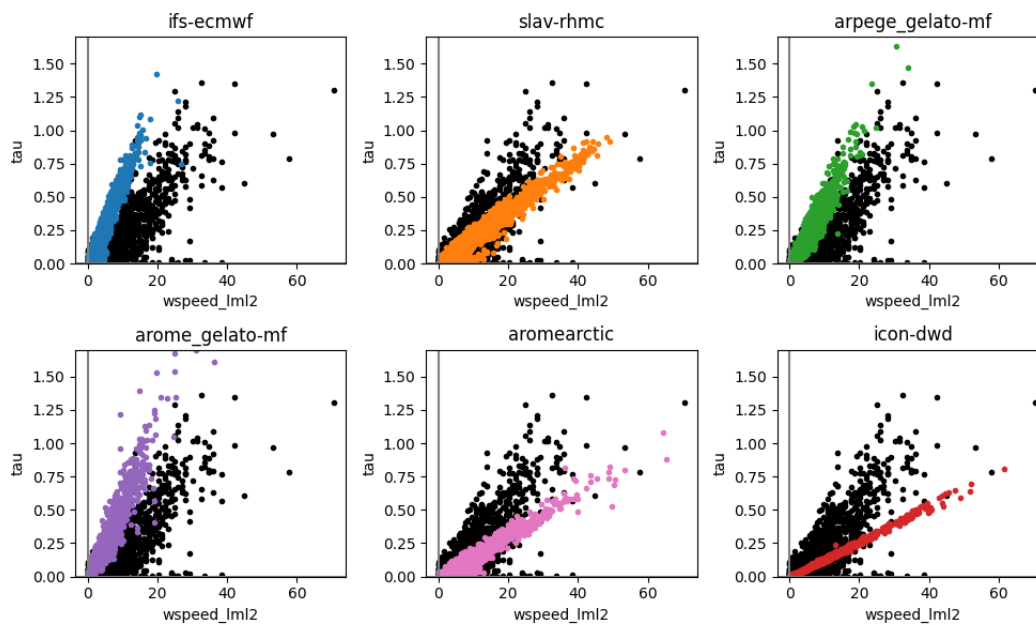


Figure 11: scatter plots of wind stress vs. the square of the near-surface (lowest model level) wind speed at Sodankylä. The observed points are shown in black and hourly values during the second day of the forecast forecast is shown in colours.

525

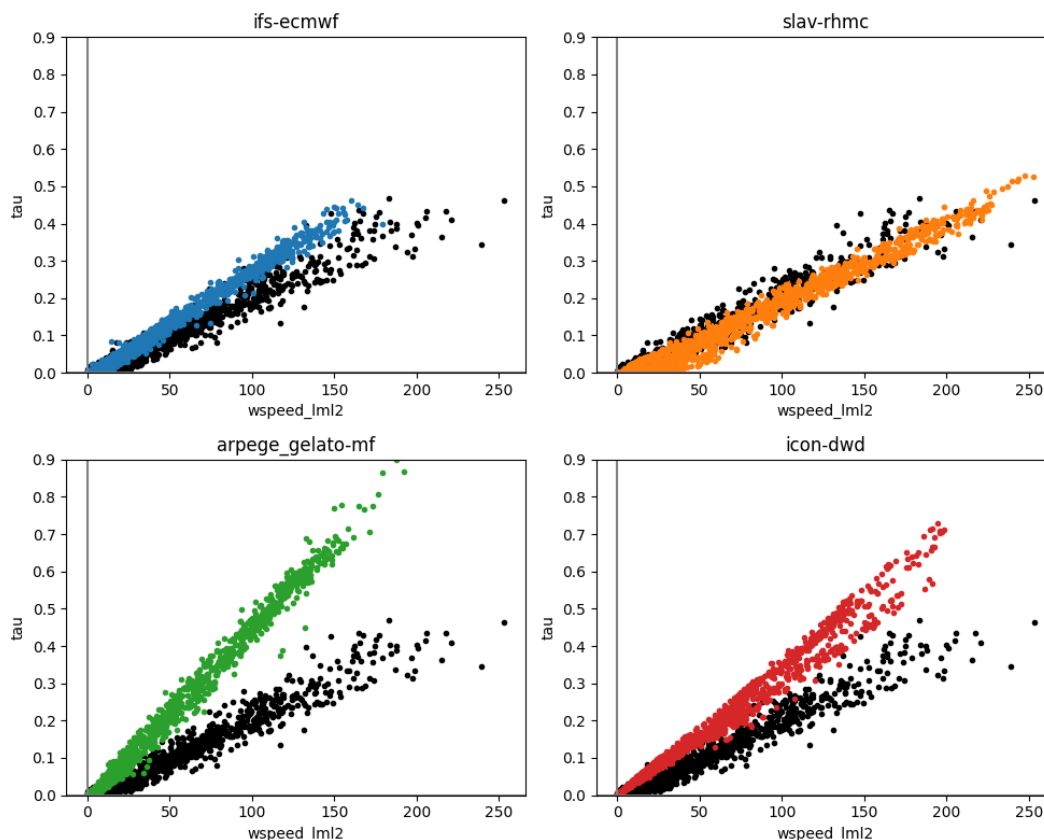


Figure 12: as Figure 11 but for Utqiagvik.

	Sodankylä	Utqiagvik
Obs	1.62	0.0012
IFS	1.82	0.0013
ARPEGE	1.50	0.0088
SLAV	1.53	0.0013
ICON-DWD	0.2	0.0070
AROME-Arctic	0.45	Outside model domain

530 **Table 4. Roughness lengths for momentum (m) at Sodankylä and Utqiagvik from observations and models.**

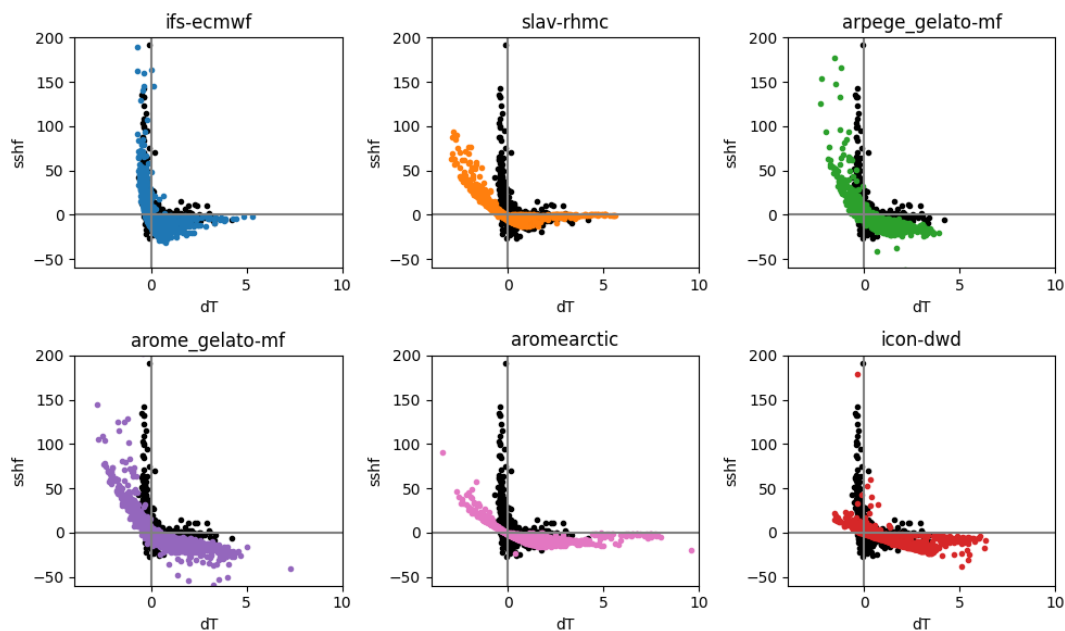
The scatterplots for the sensible heat flux (Figures 13,14) also provide some insights into the differences in the process representation between the models. The basic shape of the observed points is the same at both sites, but with fewer cases of instability at Utqiagvik compared to Sodankylä. All the models capture the link between the SHF and the temperature gradient dictated by M-O theory (see Eqn 3) however, the shape of the relationship varies between the models. For example, for the

535 ARPEGE and AROME-GELATO models the sign of the sensible heat flux does not change in a binary way with ΔT , there is spread in the location along the x-axis where this occurs. This could be due to differences in the numerical formulation of the models, i.e. the timestep at which the flux and temperature terms are stored or due to the fact that we are looking at the gridbox

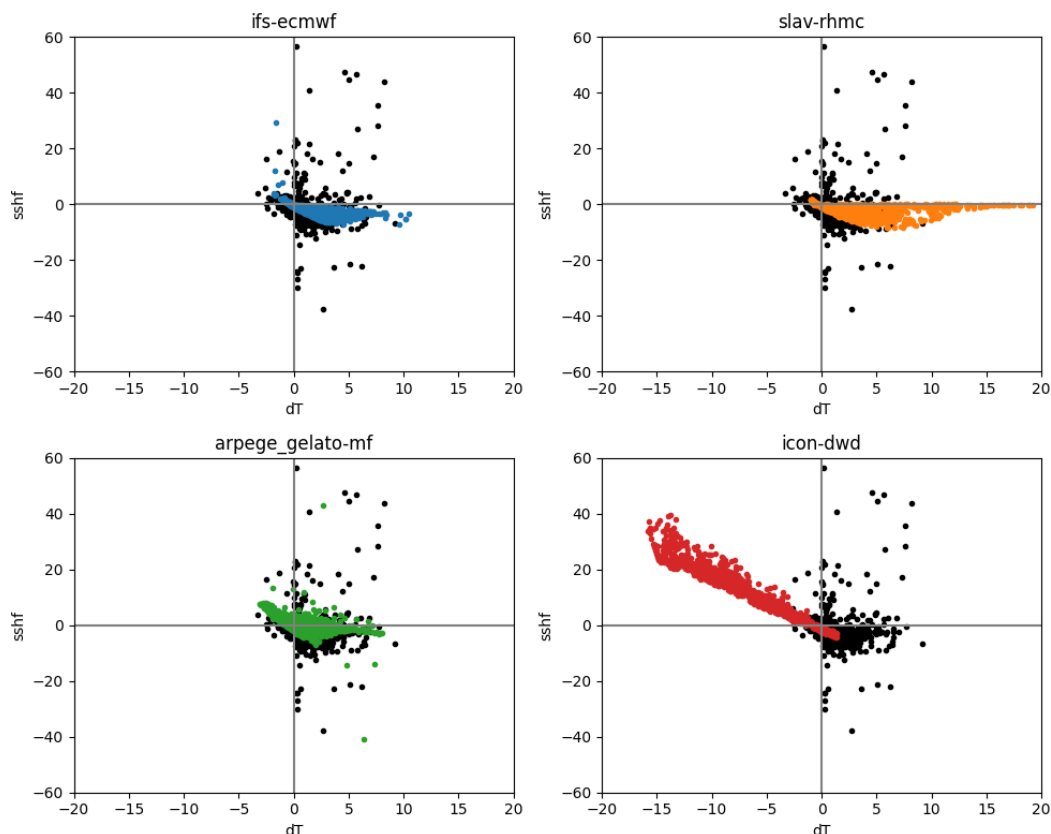


mean values where the fluxes are aggregated from values computed on different surface tiles. At Sodankylä, the IFS, SLAV and AROME-ARCTIC model have a clear tapering in the sensible heat flux towards zero for high values of ΔT . However, the
540 AROME-MF, ARPEGE and ICON do not have such a tapering and the scaled heat flux continues to grow with larger ΔT , which is qualitatively inconsistent with the observations and will lead to higher fluxes in very stable conditions inhibiting cooling of the surface. There is also a clear difference in the range of ΔT between the different models however, in the models this is an aggregate of different surface types representing forest canopy top, bare snow and frozen water and because we do not have a trustable observation of the temperature of the top of the canopy frozen water during freezing conditions it is not
545 clear what the realistic range should be.

Except for ICON, which has a large fraction of open ocean in the grid cell and therefore are biased towards convective conditions, differences between the models at Utqiagvik are less pronounced. IFS, SLAV and ARPEGE have quite a similar shape, and all underestimate the magnitude of the scaled heat flux for low values of ΔT , potentially due to the slow bias in
550 wind speeds near to the surface. Note that the large values of ΔT for the SLAV model are because the lowest model level is at $\sim 30\text{m}$, compared to $\sim 10\text{m}$ for the other models.



555 **Figure 13: scatter plots of the scaled sensible heat flux (SHF/U) vs. thermal stratification, ΔT , at Sodankylä. The observed points are shown in black and hourly values during the second day of the forecasts are shown in colours. Note that the SHF is measured at 24.5 m and for process consistency ΔT is calculated using the temperatures observed at 18m and 32m so is not directly comparable with the models.**



560

Figure 14: as Figure 13 but for Utqiagvik.

4. Conclusions and future plans

In this manuscript we have outlined the motivation for YOPPSiteMIP, documented the current status of the YOPPSiteMIP
565 forecast data archive on the YOPP data portal (hosted by MET Norway), and presented some multi-model forecast evaluation
examples to demonstrate the utility of the MMDFs and MODFs using data from the YOPP SOP1, which occurred during
February and March 2018. The main conclusions from this analysis are that:

- Near-surface temperature and wind speed forecast errors vary considerably between the different sites, reflecting both
a range of climate conditions and forecast performance across the geographies represented by this selection of sites.
- 570 • A common feature of several sites, namely Sodankylä, Barrow, Tiksi, Eureka, is a conditional warm bias during
periods of extreme cold which goes hand-in hand with a lack of temperature variability in the lowest ~100m of the
atmosphere.
- This lack of variability is investigated further at Utqiagvik, Tiksi and Sodankylä where radiation components were
observed and provided which enabled us to investigate the sensitivity of T2m to radiative forcing:
 - 575 ○ At all three sites the models tend to underestimate the sensitivity of T2m and the surface skin temperature
(or $LW\uparrow$) to variations in radiative forcing and do not capture extreme minima in these variables, although
the AROME-Arctic and CAPS models perform better in this regard.



- At Utqiagvik and Sodankylä, since turbulent fluxes were provided in addition, we were able to investigate the link between these fluxes and the bulk parameters. This highlighted:
 - the thermal representation of the land surface as an issue with all forecasts, likely due to the single-layer representation of snow used in all the forecasts submitted to YOPPsiteMIP but potentially also due to the thermal representation of forest canopy at Sodankylä.
 - Differences in the parameterisation of turbulent fluxes, particularly the specification of the roughness length for momentum which varies by a little less than an order of magnitude between different models.

585

The development of the MODFs and MMDFs is ongoing and will be completed in phases. The initial phase was to collect basic meteorology data and the main components of the radiation budget. Work on this initial phase is completed and the next phase will provide a wider range of parameters (e.g. turbulent fluxes and cloud parameters) included in the MODFs. This is a more complicated, but very necessary step since the models differ hugely in terms of surface heat and momentum fluxes as well as cloud properties (not shown). There are also plans to extend the MODF and MMDF concept to Antarctica, focussing on the Southern-hemisphere SOPs. These future phases of the YOPPsiteMIP will allow more detailed studies on e.g.:

590

- stable boundary layers, diurnal cycles and surface exchange processes,
- cloud radiative forcing and albedo,
- vertical structure of the lower atmosphere,
- assessment of cloud microphysics and hydrometeors,
- assessment of forecast models in Antarctica,
- testing of specific model developments,
- observatory representativeness.

595

This will allow a more process-focussed understanding of the forecasts in the YOPPsiteMIP archive, but also provide a testbed for model developers to use when testing new model formulations relevant for the Arctic. Further details on the MODF concept and the SOP1 and 2 MODFs can be found in Uttal et al., (2023) and Morris et al., (2023) respectively. A Python based toolkit for producing the MODFs is available on gitlab and details can be found in Gallagher et al. (manuscript in preparation).

600

Appendix A: Table of acronyms

EDMF=Eddy Diffusivity Mass Flux.

605

FE=Finite Element,

FD=Finite Difference,

FV=Finite Volume,

H=Hydrostatic,

HARATU = HARMONIE-AROME with RACMO Turbulence

610

HTESSEL=Hydrology-Tiled ECMWF Scheme for Surface Exchanges over Land,

ICE3 = Three-class ice parameterization

IQR = Inter-Quartile Range

ISBA= Interactions between Surface–Biosphere–Atmosphere,

NH=Non-hydrostatic,

615

SURFEX = Surface Externalisée,

TERRA = Land Surface module of the ICON weather forecast model.

TKE=Turbulent Kinetic Energy,



Data availability statement

All MMDF and MODFs are available on the YOPP Data Portal (<https://yopp.met.no>), hosted by the Norwegian Meteorological
620 Institute, for perpetuity (ie. longer than 10 years). The YOPP Data Portal is relying on the Arctic Data Centre
(<https://adc.met.no>) for data stewarding and the YOPPSiteMIP data can be programmatically accessed using the machine
interface for the Arctic Data Centre or can be accessed directly from
https://thredds.met.no/thredds/catalog/alertness/YOPP_supersite/obs/catalog.html, for the MODFs and
<https://thredds.met.no/thredds/catalog/YOPPSiteMIP-models/catalog.html>, for the MMDFs.

625

The SOP1 and SOP2 MODFs for each station shown in white in Fig 1 has been assigned a separate DOI, as described in Morris
et al. (submitted). In the case of the MMDFs a DOI is assigned to the data for each forecast model:

- ECMWF-IFS: <https://doi.org/10.21343/A6KA-7142>,
- ARPEGE-MF: <https://doi.org/10.21343/T31Z-J391>,
- 630 • SLAV-RHMC: <https://doi.org/10.21343/J4SJ-4N61>
- DWD-ICON: <https://doi.org/10.21343/09KM-BJ07>,
- ECCC-CAPS: <https://doi.org/10.21343/2BX6-6027>,
- AROME-MF: <https://doi.org/10.21343/JZH3-2470>,
- AROME-Arctic: <https://doi.org/10.21343/47AX-MY36>.

635

Funding

- JD was supported by European Union's Horizon 2020 Research and Innovation program through Grant Agreement
871120 (INTERACTIII).
- MT was partially supported with Russian Science Foundation, Grant 21-17-00254
- 640 • RP was supported by European Union's Horizon 2020 Research and Innovation program through Grant Agreement
101003590 (PolarRES)
- TR was supported by the Norwegian Research Council project no. 280573 'Advanced models and weather prediction
in the Arctic: enhanced capacity from observations and polar process representations (ALERTNESS)'

645 Author contributions

The initial YOPPSiteMIP, MODF and MMDF concepts were developed by GS, JD, BC, TU, SK, LMH, AS and EB. JD, BC,
EB, NA, HF, TR, RF & MT produced or ran simulations to make MMDFs. TU, EA, MG, LXH, JH, ZM, SM, EO, IS, MG, JT
and RP produced or were involved in the production of MODFs. LF, MD and ØG were responsible for the YOPPSiteMIP
archive hosted at MET Norway. JD produced the figures and wrote the manuscript with comments and input from all co-
650 authors.

Competing Interests

The authors declare that they have no conflict of interest.

655 Acknowledgements

This is a contribution to the Year of Polar Prediction (YOPP), a flagship activity of the Polar Prediction Project (PPP), initiated
by the World Weather Research Programme (WWRP) of the World Meteorological Organisation (WMO). We acknowledge
the WMO WWRP for its role in coordinating this international research activity. We would specifically like to thank Thomas
Jung, Jeff Wilson and wider PPP steering group for their tireless support of YOPPSiteMIP.



660 **References**

- Arduini, G., Balsamo, G., Dutra, E., Day, J. J., Sandu, I., Boussetta, S., & Haiden, T. (2019). Impact of a multi-layer snow scheme on near-surface weather forecasts. *Journal of Advances in Modeling Earth Systems*, 11, 4687– 4710. <https://doi.org/10.1029/2019MS001725>
- Akish, E., & Morris, S. (2023). MODF for Eureka, Canada, during YOPP SOP1 and SOP2. Norwegian Meteorological Institute. <https://doi.org/10.21343/R85J-TC61>
- Akish, E., & Morris, S. (2023). MODF for Tiksi, Russia, during YOPP SOP1 and SOP2. Norwegian Meteorological Institute. <https://doi.org/10.21343/5BWN-W881>
- Akish, E., & Morris, S. (2023). MODF for Utqiagvik, Alaska, during YOPP SOP1 and SOP2. Norwegian Meteorological Institute. <https://doi.org/10.21343/A2DX-NQ55>
- 670 Atlaskin, E. and Vihma, T.: Evaluation of NWP results for wintertime nocturnal boundary-layer temperatures over Europe and Finland, *Q. J. R. Meteorol. Soc.*, 138, 1440–1451, <https://doi.org/10.1002/qj.1885>, 2012.
- Baines, P. G., & Palmer, T. N. (1990). Rationale for a new physically-based parametrisation of sub-grid scale orographic effects. Tech. Rep. 169, European Centre for Medium-Range Weather Forecasts, Reading, UK.
- Baldauf, M., Seifert, A., Förstner, J., Majewski, D., Raschendorfer, M., & Reinhardt, T.: Operational Convective-Scale Numerical Weather Prediction with the COSMO Model: Description and Sensitivities, *Monthly Weather Review*, 139(12), 3887-3905, 2011
- 675 Balsamo, G., Beljaars, A., Scipal, K., Viterbo, P., van den Hurk, B., Hirschi, M., and Betts, A. K.: A Revised Hydrology for the ECMWF Model: Verification from Field Site to Terrestrial Water Storage and Impact in the Integrated Forecast System, *J. Hydrometeorol.*, 10, 623–643, <https://doi.org/10.1175/2008JHM1068.1>, 2009.
- 680 Batrak, Y. and Müller, M.: On the warm bias in atmospheric reanalyses induced by the missing snow over Arctic sea-ice, *Nat. Commun.*, 10, 1–8, <https://doi.org/10.1038/s41467-019-11975-3>, 2019.
- Bauer, P., Magnusson, L., Thépaut, J.-N., and Hamill, T. M.: Aspects of ECMWF model performance in polar areas, *Q. J. R. Meteorol. Soc.*, 142, 583–596, <https://doi.org/10.1002/qj.2449>, 2016.
- 685 Bazile, E., & Azouz, N. (2023a). Merged model Data Files (MMDFs) for the Meteo France ARPEGE global forecast model for various Polar sites. Norwegian Meteorological Institute. <https://doi.org/10.21343/T31Z-J391>
- Bazile, E., & Azouz, N. (2023b). MMDFs for the Meteo France AROME regional forecast model for various Arctic sites. Norwegian Meteorological Institute. <https://doi.org/10.21343/JZH3-2470>
- E.Bazile, N. Azouz, A. Napoly, C. Loo: Impact of the 1D sea-ice model GELATO in the global model ARPEGE. France
- 690 6-03. http://bluebook.meteoinfo.ru/index.php?year=2020&ch_=2
- Bazile, E., Marquet, P., Bouteloup, Y, and Bouyssel, F.: The Turbulent Kinetic Energy (TKE) scheme in the NWP models at Météo-France, ECMWF GABLS Workshop on Diurnal cycles and the stable boundary layer, 7-10 November 2011
- 695 Bélair, S., Brown, R., Mailhot, J., Bilodeau, B., & Crevier, L. (2003). Operational Implementation of the ISBA Land Surface Scheme in the Canadian Regional Weather Forecast Model. Part II: Cold Season Results, *Journal of Hydrometeorology*, 4(2), 371-386.
- Bélair, S., J. Mailhot, C. Girard, and P. Vaillancourt, 2005: Boundary Layer and Shallow Cumulus Clouds in a Medium-Range Forecast of a Large-Scale Weather System. *Mon. Wea. Rev.*, 133, 1938–1960, <https://doi.org/10.1175/MWR2958.1>.
- 700 Beljaars, A. C. M. and Holtlag, A. a. M.: Flux Parameterization over Land Surfaces for Atmospheric Models, *J. Appl. Meteorol.*, 30, 327–341, [https://doi.org/10.1175/1520-0450\(1991\)030<0327:FPOLSF>2.0.CO;2](https://doi.org/10.1175/1520-0450(1991)030<0327:FPOLSF>2.0.CO;2), 1991.
- Bengtsson, L., Andrae, U., Aspelién, T., Batrak, Y., Calvo, J., Rooy, W. de, Gleeson, E., Hansen-Sass, B., Homleid, M., Hortal, M., Ivarsson, K.-I., Lenderink, G., Niemelä, S., Nielsen, K. P., Onvlee, J., Rontu, L., Samuelsson, P., Muñoz, D. S., Subias,



- 705 A., Tijm, S., Toll, V., Yang, X., and Køltzow, M. Ø.: The HARMONIE–AROME Model Configuration in the ALADIN–HIRLAM NWP System, *Mon. Weather Rev.*, 145, 1919–1935, <https://doi.org/10.1175/MWR-D-16-0417.1>, 2017.
- Bechtold, P., M. Köhler, T. Jung, F. Doblas-Reyes, M. Leutbecher, M. J. Rodwell, F. Vitart, and G. Balsamo, 2008: Advances in simulating atmospheric variability with the ECMWF model: From synoptic to decadal time-scales. *Quarterly Journal of the Royal Meteorological Society*, 134 (634), 1337–1351, <https://doi.org/10.1002/qj.289>, URL <https://onlinelibrary.wiley.com/doi/10.1002/qj.289>.
- 710 Bechtold, P., E. Bazile, F. Guichard, P. Mascart and E. Richard, 2001 : A mass flux convection scheme for regional and global models. *Quart. J. Roy. Meteor. Soc.*, 127, 869-886.
- Bélair, S., Brown, R., Mailhot, J., Bilodeau, B., & Crevier, L. (2003). Operational Implementation of the ISBA Land Surface Scheme in the Canadian Regional Weather Forecast Model. Part II: Cold Season Results, *Journal of Hydrometeorology*, 4(2), 371-386.
- 715 Belair et al., 2005: Boundary Layer and Shallow Cumulus Clouds in a Medium-Range Forecast of a Large-Scale Weather System. *Monthly Weather Review*, Vol. 133, 1938-1960
- Bougeault, P.: Cloud ensemble relations for use in higher order models of the planetary boundary layer, *J. Atmos. Sci.*, 39, 2691-2700, 1982.
- Bougeault, P. (1985). A simple parameterisation of the large scale effects of cumulus convection. *Mon. Wea. Rev.*, 4:469–485.
- 720 Bromwich, D. H., Werner, K., Casati, B., Powers, J. G., Gorodetskaya, I. V., Massonnet, F., Vitale, V., Heinrich, V. J., Liggett, D., Arndt, S., Barja, B., Bazile, E., Carpentier, S., Carrasco, J. F., Choi, T., Choi, Y., Colwell, S. R., Cordero, R. R., Gervasi, M., Haiden, T., Hirasawa, N., Inoue, J., Jung, T., Kalesse, H., Kim, S.-J., Lazzara, M. A., Manning, K. W., Norris, K., Park, S.-J., Reid, P., Rigor, I., Rowe, P. M., Schmithüsen, H., Seifert, P., Sun, Q., Uttal, T., Zannoni, M., and Zou, X.: The Year of Polar Prediction in the Southern Hemisphere (YOPP-SH), *Bull. Am. Meteorol. Soc.*, 101, E1653–E1676, <https://doi.org/10.1175/BAMS-D-19-0255.1>, 2020.
- 725 Buizza, R., Bidlot, J.-R., Janousek, M., Keeley, S., Mogensen, K., and Richardson, D.: New IFS cycle brings sea-ice coupling and higher ocean resolution, *ECMWF Newsl. - Number 150*, 14–17, <https://doi.org/10.21957/xbov3ybily>, 2017.
- Casati, B. (2023). MMDFs for the Environment and Climate Change Canada-CAPS regional forecast model for various Arctic sites. Norwegian Meteorological Institute. <https://doi.org/10.21343/2BX6-6027>
- 730 Casati, B., T. Robinson, F. Lemay, M. Køltzow, T. Haiden, E. Mekis, F. Lespinas, V. Fortin, G. Gascon, J. Milbrandt, G. Smith (2023) Performance of the Canadian Arctic Prediction System during the YOPP Special Observing Periods. *Atmosphere-Ocean*, <https://doi.org/10.1080/07055900.2023.2191831>
- Casati, B.: Model process-based evaluation using high-frequency multi-variate observations at the Arctic and Antarctic supersites during the Year of Polar Prediction: the YOPPsiteMIP, n.d.
- 735 Catry, B., Geleyn, J. F., Bouyssel, F., Cedilnik, J., Brožková, R., & Derková, M. (2008). A new sub-grid scale lift formulation in a mountain drag parameterisation scheme. *Meteorologische Zeitschrift*, 17(2), 193–208. <https://doi.org/10.1127/0941-2948/2008/0272>
- Cheng, Y., V. M. Canuto, and A. M. Howard, 2002: An Improved Model for the Turbulent PBL. *J. Atmos. Sci.*, 59, 1550–1565, [https://doi.org/10.1175/1520-0469\(2002\)059<1550:AIMFTT>2.0.CO;2](https://doi.org/10.1175/1520-0469(2002)059<1550:AIMFTT>2.0.CO;2).
- 740 Coté, J., S. Gravel, A. Méthot, A. Patoine, M. Roch, and A. Staniforth, 1998: The operational CMC–MRD Global Environmental Multiscale (GEM) model. Part I: Design considerations and formulation. *Mon. Wea. Rev.*, 126, 1373–1395, doi:10.1175/1520-0493(1998)126,1373:TOCMGE.2.0.CO;2.
- Curry, J.: On the Formation of Continental Polar Air, *J. Atmospheric Sci.*, 40, 2278–2292, [https://doi.org/10.1175/1520-0469\(1983\)040<2278:OTFOCP>2.0.CO;2](https://doi.org/10.1175/1520-0469(1983)040<2278:OTFOCP>2.0.CO;2), 1983.
- 745 Cuxart, J., Bougeault, P. and Redelsperger, J.-L. (2000), A turbulence scheme allowing for mesoscale and large-eddy simulations. *Q.J.R. Meteorol. Soc.*, 126: 1-30. <https://doi.org/10.1002/qj.49712656202>
- Cuxart, J., Holtslag, A. A. M., Beare, R. J., Bazile, E., Beljaars, A., Cheng, A., Conangla, L., Ek, M., Freedman, F., Hamdi, R., Kerstein, A., Kitagawa, H., Lenderink, G., Lewellen, D., Mailhot, J., Mauritsen, T., Perov, V., Schayes, G., Steeneveld,



- G.-J., Svensson, G., Taylor, P., Weng, W., Wunsch, S., and Xu, K.-M.: Single-Column Model Intercomparison for a Stably Stratified Atmospheric Boundary Layer, *Boundary-Layer Meteorol.*, 118, 273–303, <https://doi.org/10.1007/s10546-005-3780-1>, 2006.
- Day, J. (2023). MMDFs for the ECMWF-IFS global forecast model for various Polar sites. Norwegian Meteorological Institute. <https://doi.org/10.21343/A6KA-7142>
- Day, J. J., Sandu, I., Magnusson, L., Rodwell, M. J., Lawrence, H., Bormann, N., and Jung, T.: Increased Arctic influence on the midlatitude flow during Scandinavian Blocking episodes, *Q. J. R. Meteorol. Soc.*, 145, 3846–3862, <https://doi.org/10.1002/qj.3673>, 2019.
- Day, J. J., Arduini, G., Sandu, I., Magnusson, L., Beljaars, A., Balsamo, G., Rodwell, M., and Richardson, D.: Measuring the Impact of a New Snow Model Using Surface Energy Budget Process Relationships, *J. Adv. Model. Earth Syst.*, 12, <https://doi.org/10.1029/2020MS002144>, 2020.
- 760 Day, J. J., Keeley, S., Arduini, G., Magnusson, L., Mogensen, K., Rodwell, M., Sandu, I., and Tietsche, S.: Benefits and challenges of dynamic sea ice for weather forecasts, *Weather Clim. Dyn.*, 3, 713–731, <https://doi.org/10.5194/wcd-3-713-2022>, 2022.
- Delage, Y. (1997): Parametrizing sub-grid scale vertical transport in atmospheric models under statically stable conditions. *Boundary-Layer Meteorology* 82, 23–48 (1997). <https://doi.org/10.1023/A:1000132524077>
- 765 Delage, Y., and C. Girard (1992): Stability functions correct at the free convection limit and consistent for both the surface and Ekman layers. *Boundary-Layer Meteorol* 58, 19–31. <https://doi.org/10.1007/BF00120749>
- Donlon, C. J., Martin, M., Stark, J., Roberts-Jones, J., Fiedler, E., and Wimmer, W.: The Operational Sea Surface Temperature and Sea Ice Analysis (OSTIA) system, *Remote Sens. Environ.*, 116, 140–158, <https://doi.org/10.1016/j.rse.2010.10.017>, 2012.
- Đurán, I. B., J. Geleyn, F. Váňa, J. Schmidli, and R. Brožková, 2018: A Turbulence Scheme with Two Prognostic Turbulence Energies. *J. Atmos. Sci.*, 75, 3381–3402, <https://doi.org/10.1175/JAS-D-18-0026.1>.
- 770 Dyer, A. J. (1974). A review of flux-profile relationships. *Boundary-Layer Meteorol.*, 7, 363–372.
- Emmerson, C., and G. Lahn, 2012: Arctic opening: Opportunity and risk in the high north. *Lloyds Rep.*, 59 pp. [Available online at www.chathamhouse.org/sites/files/chathamhouse/public/Research/Energy,%20Environment%20and%20Development/0412arctic.pdf]
- 775 Forbes, R. M. and Ahlgrimm, M.: On the Representation of High-Latitude Boundary Layer Mixed-Phase Cloud in the ECMWF Global Model, *Mon. Weather Rev.*, 142, 3425–3445, <https://doi.org/10.1175/MWR-D-13-00325.1>, 2014.
- Frank, H. (2023). MMDFs for the DWD-ICON global forecast model for various Arctic sites. Norwegian Meteorological Institute. <https://doi.org/10.21343/09KM-BJ07>
- 780 Gerard, L. and Geleyn, J.-F. (2005), Evolution of a subgrid deep convection parametrization in a limited-area model with increasing resolution. *Q.J.R. Meteorol. Soc.*, 131: 2293-2312. <https://doi.org/10.1256/qj.04.72>
- Gerard, L., J. Piriou, R. Brožková, J. Geleyn, and D. Banciu, 2009: Cloud and Precipitation Parameterization in a Meso-Gamma-Scale Operational Weather Prediction Model. *Mon. Wea. Rev.*, 137, 3960–3977, <https://doi.org/10.1175/2009MWR2750.1>.
- 785 Girard, C., and Coauthors, 2014: Staggered vertical discretization of the Canadian Environmental Multiscale (GEM) model using a coordinate of the log-hydrostatic-pressure type. *Mon. Wea. Rev.*, 142, 1183–1196, doi:10.1175/MWR-D-13-00255.1.
- Goessling, H. F., and Coauthors, 2016: Paving the way for the Year of Polar Prediction. *Bull. Amer. Meteor. Soc.*, 97, ES85–ES88, doi:10.1175/BAMS-D-15-00270.1.
- Haiden, T., Sandu, I., Balsamo, G., Arduini, G., and Beljaars, A.: Addressing biases in near-surface forecasts, ECMWF, <https://doi.org/10.21957/eng71d53th>, 2018.
- 790 Hartten, L. M. and Khalsa, S. J. S.: The H-K Variable SchemaTable developed for the YOPPsiteMIP, <https://doi.org/10.5281/zenodo.6463464>, 2022.



- Heise E., Ritter B. & Schrodin R. 2006. Operational implementation of the multilayer soil model. COSMO Technical Reports No. 9. Offenbach am Main, Germany: Consortium for Small-Scale Modelling.
- 795 Hogan, R. J. and Bozzo, A.: A Flexible and Efficient Radiation Scheme for the ECMWF Model, *J. Adv. Model. Earth Syst.*, 10, 1990–2008, <https://doi.org/10.1029/2018MS001364>, 2018.
- Högström, U. (1988). Non-dimensional wind and temperature profiles in the atmospheric surface layer: A re-evaluation. *Boundary-Layer Meteorol.*, 42, 55–78.
- Holt, J. (2023). Merged Observatory Data File (MODF) for Ny Alesund. Norwegian Meteorological Institute.
- 800 <https://doi.org/10.21343/Y89M-6393>
- Holtstag, A. A. M., & De Bruin, H. A. R. (1988). Applied Modeling of the Nighttime Surface Energy Balance over Land, *Journal of Applied Meteorology and Climatology*, 27(6), 689-704.
- Holtstag, A. A. M., Svensson, G., Baas, P., Basu, S., Beare, B., Beljaars, A. C. M., Bosveld, F. C., Cuxart, J., Lindvall, J., Steeneveld, G. J., Tjernström, M., & Van De Wiel, B. J. H. (2013). Stable Atmospheric Boundary Layers and Diurnal Cycles: Challenges for Weather and Climate Models, *Bulletin of the American Meteorological Society*, 94(11), 1691-1706.
- 805 Iacono, M., Delamere, J., Mlawer, E., Shephard, M., Clough, S. and Collins, W. (2008). Radiative forcing by long-lived greenhouse gases: Calculations with the AER radiative transfer models. *J. Geophys. Res.*, 113D, 13103.
- Huang, L., Mariani, Z., & Crawford, R. (2023). MODF for Iqaluit Airport, Iqaluit, Nunavut, Canada during YOPP SOP1 and SOP2. Norwegian Meteorological Institute. <https://doi.org/10.21343/YRNF-CK57>
- 810 Huang, L., Mariani, Z., & Crawford, R. (2023). MODF for Erik Nielsen Airport, Whitehorse, Canada during YOPP SOP1 and SOP2. Norwegian Meteorological Institute. <https://doi.org/10.21343/A33E-J150>
- Illingworth, A. J., Hogan, R. J., O'Connor, E. J., Bouniol, D., Brooks, M. E., Delanoé, J., Donovan, D. P., Eastment, J. D., Gaussiat, N., Goddard, J. W. F., Haefelin, M., Baltink, H. K., Krasnov, O. A., Pelon, J., Piriou, J.-M., Protat, A., Russchenberg, H. W. J., Seifert, A., Tompkins, A. M., van Zadelhoff, G.-J., Vinit, F., Willén, U., Wilson, D. R., and Wrench, C. L.: Cloudnet, *Bull. Am. Meteorol. Soc.*, 88, 883–898, <https://doi.org/10.1175/BAMS-88-6-883>, 2007.
- 815 Jung, T., Gordon, N. D., Bauer, P., Bromwich, D. H., Chevallier, M., Day, J. J., Dawson, J., Doblas-Reyes, F., Fairall, C., Goessling, H. F., Holland, M., Inoue, J., Iversen, T., Klebe, S., Lemke, P., Losch, M., Makshtas, A., Mills, B., Nurmi, P., Perovich, D., Reid, P., Renfrew, I. A., Smith, G., Svensson, G., Tolstykh, M., and Yang, Q.: Advancing Polar Prediction Capabilities on Daily to Seasonal Time Scales, *Bull. Am. Meteorol. Soc.*, 97, 1631–1647, <https://doi.org/10.1175/BAMS-D-14-00246.1>, 2016.
- 820 Karlsson J. and G. Svensson, 2013: Consequences of poor representation of Arctic sea-ice albedo and cloud-radiation interactions in the CMIP5 model ensemble. *Geophys. Res. Lett.*, 40, 4374–4379, doi:10.1002/grl.50768
- Koltzow, M., Casati, B., Bazile, E., Haiden, T., and Valkonen, T.: An NWP Model Intercomparison of Surface Weather Parameters in the European Arctic during the Year of Polar Prediction Special Observing Period Northern Hemisphere 1, *Weather Forecast.*, 34, 959–983, <https://doi.org/10.1175/WAF-D-19-0003.1>, 2019.
- 825 Köhler, M., Ahlgrimm, M. and Beljaars, A. (2011). Unified treatment of dry convective and stratocumulus topped boundary layers in the ECMWF model. *Q. J. R. Meteorol. Soc.*, 137, 43–57.
- Lawrence, H., Bormann, N., Sandu, I., Day, J., Farnan, J., and Bauer, P.: Use and impact of Arctic observations in the ECMWF Numerical Weather Prediction system, *Q. J. R. Meteorol. Soc.*, 145, 3432–3454, <https://doi.org/10.1002/qj.3628>, 2019.
- 830 Lenderink, G. and Holtstag, A.A.M. (2004), An updated length-scale formulation for turbulent mixing in clear and cloudy boundary layers. *Q.J.R. Meteorol. Soc.*, 130: 3405-3427. <https://doi.org/10.1256/qj.03.117>
- Li, J. and H.W Barker, 2005: A radiation algorithm with correlated-k distribution. Part I: Local thermal equilibrium. *J. Atmos. Sci.*, 62, 286-309.
- Lott, F. and Miller, M. J. (1997). A new subgrid-scale orographic drag parametrization: Its formulation and testing. *Q. J. R. Meteorol. Soc.*, 123, 101–127.
- 835 Louis, J. F.: A parametric model of vertical eddy fluxes in the atmosphere | SpringerLink, *Bound.-Layer Meteorol.*, 1979.



- Masson, V., Le Moigne, P., Martin, E., Faroux, S., Alias, A., Alkama, R., Belamari, S., Barbu, A., Boone, A., Bouysse, F., Brousseau, P., Brun, E., Calvet, J.-C., Carrer, D., Decharme, B., Delire, C., Donier, S., Essauini, K., Gibelin, A.-L., Giordani, H., Habets, F., Jidane, M., Kerdraon, G., Kourzeneva, E., Lafaysse, M., Lafont, S., Lebeaupin Brossier, C., Lemonsu, A.,
840 Mahfouf, J.-F., Marguinaud, P., Mokhtari, M., Morin, S., Pigeon, G., Salgado, R., Seity, Y., Taillefer, F., Tanguy, G., Tulet, P., Vincendon, B., Vionnet, V., and Voldoire, A.: The SURFEXv7.2 land and ocean surface platform for coupled or offline simulation of earth surface variables and fluxes, *Geosci. Model Dev.*, 6, 929–960, <https://doi.org/10.5194/gmd-6-929-2013>, 2013.
- Milbrandt, J. A. and Morrison, H.: Parameterization of Cloud Microphysics Based on the Prediction of Bulk Ice Particle Properties. Part III: Introduction of Multiple Free Categories, *J. Atmospheric Sci.*, 73, 975–995, <https://doi.org/10.1175/JAS-D-15-0204.1>, 2016.
- Milbrandt, J. A., Bélair, S., Faucher, M., Vallée, M., Carrera, M. L., and Glazer, A.: The Pan-Canadian High Resolution (2.5 km) Deterministic Prediction System, *Weather Forecast.*, 31, 1791–1816, <https://doi.org/10.1175/WAF-D-16-0035.1>, 2016.
- Miller, N. B., Shupe, M. D., Cox, C. J., Noone, D., Persson, P. O. G., and Steffen, K.: Surface energy budget responses to radiative forcing at Summit, Greenland, *The Cryosphere*, 11, 497–516, <https://doi.org/10.5194/tc-11-497-2017>, 2017.
- Miller, N. B., Shupe, M. D., Lenaerts, J. T. M., Kay, J. E., de Boer, G., & Bennartz, R. (2018). Process-based model evaluation using surface energy budget observations in central Greenland. *Journal of Geophysical Research: Atmospheres*, 123, 4777–4796. <https://doi.org/10.1029/2017JD027377>
- Mlawer, E. J., Taubman, S. J., Brown, P. D., Iacono, M. J. and Clough, S. A. (1997). Radiative transfer for inhomogeneous atmospheres: RRTM, a validated correlated-k model for the longwave. *J. Geophys. Res.*, 102D, 16663–16682.
- Morris et al. (submitted to ESSD): Special Observing Period (SOP) Data for the Year of Polar Prediction site Model Intercomparison Project (YOPPsiteMIP)
- Morrison, H. and Milbrandt, J. A.: Parameterization of Cloud Microphysics Based on the Prediction of Bulk Ice Particle Properties. Part I: Scheme Description and Idealized Tests, *J. Atmospheric Sci.*, 72, 287–311, <https://doi.org/10.1175/JAS-D-14-0065.1>, 2015.
- Morrison, H., Milbrandt, J. A., Bryan, G. H., Ikeda, K., Tessendorf, S. A., and Thompson, G.: Parameterization of Cloud Microphysics Based on the Prediction of Bulk Ice Particle Properties. Part II: Case Study Comparisons with Observations and Other Schemes, *J. Atmospheric Sci.*, 72, 312–339, <https://doi.org/10.1175/JAS-D-14-0066.1>, 2015.
- Müller, M., and Coauthors, 2017: AROME-MetCoOp: A Nordic Convective-Scale Operational Weather Prediction Model. *Wea. Forecasting*, 32, 609–627, <https://doi.org/10.1175/WAF-D-16-0099.1>.
- Noilhan, J., & Planton, S. (1989). A Simple Parameterization of Land Surface Processes for Meteorological Models, *Monthly Weather Review*, 117(3), 536–549.
- O'Connor, E. (2023). Merged observation data file for Sodankyla. Norwegian Meteorological Institute. <https://doi.org/10.21343/M16P-PQ17>
- 870 Pailleux, J., Geleyn, J.-F., Hamrud, M., Courtier, P., Thépaut, J.-N., Rabier, F., Andersson, E., Burridge, D., Simmons, A., Salmond, D., Khatib, E., and Fischer, C.: Twenty-five years of IFS/ARPEGE, <https://doi.org/10.21957/FTU6MFVY>, 2014.
- Pergaud, J., Masson, V., Malardel, S. et al. A Parameterization of Dry Thermals and Shallow Cumuli for Mesoscale Numerical Weather Prediction. *Boundary-Layer Meteorol* 132, 83–106 (2009). <https://doi.org/10.1007/s10546-009-9388-0>
- 875 Pinty, J.-P. and P. Jabouille (1998), A mixed-phase cloud parameterization for use in a mesoscale non-hydrostatic model: Simulations of a squall line and of orographic precipitation, *Proc. Conf. on Cloud Physics*, 217–220.
- Pithan, F., Medeiros, B., and Mauritsen, T.: Mixed-phase clouds cause climate model biases in Arctic wintertime temperature inversions, *Clim. Dyn.*, 43, 289–303, <https://doi.org/10.1007/s00382-013-1964-9>, 2014.
- 880



- Pithan, F., Ackerman, A., Angevine, W. M., Hartung, K., Ickes, L., Kelley, M., Medeiros, B., Sandu, I., Steeneveld, G.-J., Sterk, H. a. M., Svensson, G., Vaillancourt, P. A., and Zadra, A.: Select strengths and biases of models in representing the Arctic winter boundary layer over sea ice: the Larcform 1 single column model intercomparison, *J. Adv. Model. Earth Syst.*, 8, 1345–1357, <https://doi.org/10.1002/2016MS000630>, 2016.
- 885 Prill, F., Reinert, D., Rieger, D., Zängl, G.: ICON Tutorial - Working with the ICON model, https://doi.org/10.5676/dwd_pub/nwv/icon_tutorial2020, 2020
Raschendorfer, M., 2001: The new turbulence parameterization of LM. *COSMO Newsl.*, 1, 89–97.
Remes, T. (2023). MMDFs for the MetNorway AROME regional forecast model for various Arctic sites. Norwegian Meteorological Institute. <https://doi.org/10.21343/47AX-MY36>
- 890 Rodwell, M. J. and Palmer, T. N.: Using numerical weather prediction to assess climate models, *Q. J. R. Meteorol. Soc.*, 133, 129–146, <https://doi.org/10.1002/qj.23>, 2007.
- Roehrig, R., Beau, I., Saint-Martin, D., Alias, A., Decharme, B., Guérémy, J.-F., Voldoire, A., Abdel-Lathif, A. Y., Bazile, E., Belamari, S., Blein, S., Bouniol, D., Bouteloup, Y., Cattiaux, J., Chauvin, F., Chevallier, M., Colin, J., Douville, H., Marquet, P., Michou, M., Nabat, P., Oudar, T., Peyrillé, P., Piriou, J.-M., Salas y Méria, D., Sférian, R., and Sénéci, S.: The CNRM Global Atmosphere Model ARPEGE-Climat 6.3: Description and Evaluation, *J. Adv. Model. Earth Syst.*, 12, e2020MS002075, <https://doi.org/10.1029/2020MS002075>, 2020.
- 895 Sandu, I., Beljars, A., Bechtold, P., Mauritsen, T., and Balsamo, G.: Why is it so difficult to represent stably stratified conditions in numerical weather prediction (NWP) models?, *J. Adv. Model. Earth Syst.*, 5, 117–133, <https://doi.org/10.1002/jame.20013>, 2013.
- 900 Sedlar, J., Tjernström, M., Rinke, A., Orr, A., Cassano, J., Fettweis, X., et al. (2020). Confronting Arctic troposphere, clouds, and surface energy budget representations in regional climate models with observations. *Journal of Geophysical Research: Atmospheres*, 125. <https://doi.org/10.1029/2019JD031783>
- Seity, Y., Brousseau, P., Malardel, S., Hello, G., Bénard, P., Bouttier, F., Lac, C., and Masson, V.: The AROME-France Convective-Scale Operational Model, *Mon. Weather Rev.*, 139, 976–991, <https://doi.org/10.1175/2010MWR3425.1>, 2011.
- 905 Seity, Y., Lac, C., Bouyssel, F., Riette, S., & Bouteloup, Y. (2012, November). Cloud and microphysical schemes in ARPEGE and AROME models. In *Proceedings of the Workshop on Parametrization of Clouds and Precipitation (ECMWF)*, Reading, UK (pp. 5-8).
Seifert, A.: A revised cloud microphysical parameterization for COSMO-LME. *COSMO News Letter No. 7*, <http://www.cosmo-model.org>, 2008
- 910 Shupe, M.D., Rex, M., Blomquist, B., Persson, P.O.G., Schmale, J., Uttal, T., Althausen, D., Angot, H., Archer, S., Bariteau, L. and Beck, I., 2022. Overview of the MOSAiC expedition: Atmosphere. *Elem Sci Anth*, 10(1), p.00060.
Solomon, A., Shupe, M.D., Svensson, G., Barton, N.P., Batrak, Y., Bazile, E., Day, J.J., Doyle, J.D., Frank, H.P., Keeley, S., Remes, T., and Tolstykh, M., 2023. The Winter Central Arctic Surface Energy Budget; A Model Evaluation using Observations from the MOSAiC Campaign. *Elem Sci Anth*, in press.
- 915 Soares, P., P. Miranda, A. Siebesma, and J. Teixeira, 2004: An eddy-diffusivity/mass-flux parametrization for dry and shallow cumulus convection. *Quart. J. Roy. Meteor. Soc.*, 130, 3365–3383, doi:10.1256/qj.03.223.
Siebesma, A. P., P. M. Soares, and J. Teixeira, 2007: A combined eddy diffusivity mass-flux approach for the convective boundary layer. *J. Atmos. Sci.*, 64, 1230–1248, doi:10.1175/JAS3888.1.
Svensson, G. and Karlsson, J.: On the Arctic Wintertime Climate in Global Climate Models, *J. Clim.*, 24, 5757–5771, <https://doi.org/10.1175/2011JCLI4012.1>, 2011.
- 920 Tarasova, T. A., and B. A. Fomin, 2007: The Use of New Parameterizations for Gaseous Absorption in the CLIRAD-SW Solar Radiation Code for Models. *J. Atmos. Oceanic Technol.*, 24, 1157–1162, <https://doi.org/10.1175/JTECH2023.1>.
Tiedtke, M., 1993: Representation of Clouds in Large-Scale Models. *Monthly Weather Review*, 121 (11), 3040–3061,



- 925 Tjernström, M., Žagar, M., Svensson, G., Cassano, J. J., Pfeifer, S., Rinke, A., Wyser, K., Dethloff, K., Jones, C., Semmler, T., and Shaw, M.: ‘Modelling the Arctic Boundary Layer: An Evaluation of Six Arcmip Regional-Scale Models using Data from the Sheba Project,’ *Bound.-Layer Meteorol.*, 117, 337–381, <https://doi.org/10.1007/s10546-004-7954-z>, 2005.
- Tjernström, M., Svensson, G., Magnusson, L., Brooks, I. M., Prytherch, J., Vüllers, J., and Young, G.: Central Arctic weather forecasting: Confronting the ECMWF IFS with observations from the Arctic Ocean 2018 expedition, *Q. J. R. Meteorol. Soc.*, 147, 1278–1299, <https://doi.org/10.1002/qj.3971>, 2021.
- 930 Tolstykh, M. (2023). MMDFs for the Roshydromet-SLAV global forecast model for various Arctic sites. Norwegian Meteorological Institute. <https://doi.org/10.21343/J4SJ-4N61>
- Tolstykh, M. A., Fadeev, R. Yu., Shashkin, V. V., Goyman, G. S., Zaripov, R. B., Kiktev, D. B., Makhnorylova, S. V., Mizyak, V. G., and Rogutov, V. S.: Multiscale Global Atmosphere Model SLAV: the Results of Medium-range Weather Forecasts, *Russ. Meteorol. Hydrol.*, 43, 773–779, <https://doi.org/10.3103/S1068373918110080>, 2018.
- 935 Uttal, T., Starkweather, S., Drummond, J. R., Vihma, T., Makshtas, A. P., Darby, L. S., Burkhart, J. F., Cox, C. J., Schmeisser, L. N., Haiden, T., Maturilli, M., Shupe, M. D., De Boer, G., Saha, A., Grachev, A. A., Crepinsek, S. M., Bruhwiler, L., Goodison, B., McArthur, B., Walden, V. P., Dlugokencky, E. J., Persson, P. O. G., Lesins, G., Laurila, T., Ogren, J. A., Stone, R., Long, C. N., Sharma, S., Massling, A., Turner, D. D., Stanitski, D. M., Asmi, E., Aurela, M., Skov, H., Eleftheriadis, K., Virkkula, A., Platt, A., Förland, E. J., Iijima, Y., Nielsen, I. E., Bergin, M. H., Candlish, L., Zimov, N. S., Zimov, S. A., O’Neill, N. T., Fogal, P. F., Kivi, R., Konopleva-Akish, E. A., Verlinde, J., Kustov, V. Y., Vasel, B., Ivakhov, V. M., Viisanen, Y., and Intrieri, J. M.: International Arctic Systems for Observing the Atmosphere: An International Polar Year Legacy Consortium, *Bull. Am. Meteorol. Soc.*, 97, 1033–1056, <https://doi.org/10.1175/BAMS-D-14-00145.1>, 2015.
- Uttal, T. L.M. Hartten, S.J. Khalsa, B. Casati, G. Svensson, J. Day, M. Gallagher, J. Holt, E. Aksh, S. Morris, E. O’Connor, R. Pirazzini, L. Huang, R. Crawford, Z. Mariani, O. Godoy, J. A.K. Tjernstrom, G. Prakesh, N. Hickmon, M. Maturilli, and
- 945 C. Cox, Merged Observatory Data Files (MODFs): An Integrated Research Data Product Supporting Process Oriented Investigations and Diagnostics. 2023.
- Van de Wiel, B. J. H., Vignon, E., Baas, P., van Hooijdonk, I. G. S., van der Linden, S. J. A., Antoon van Hooft, J., Bosveld, F. C., de Roode, S. R., Moene, A. F., & Genthon, C. (2017). Regime Transitions in Near-Surface Temperature Inversions: A Conceptual Model, *Journal of the Atmospheric Sciences*, 74(4), 1057-1073. doi: <https://doi.org/10.1175/JAS-D-16-0180.1>
- 950 van Meijgaard, E., L. van Ulft, G. Lenderink, S. De Roode, E. L. Wipfler, R. Boers, and R. van Timmermans, 2012: Refinement and application of a regional atmospheric model for climate scenario calculations of Western Europe. KVR Research Rep. 054/12, 44 pp. [Available online at <http://library.wur.nl/WebQuery/wurpubs/fulltext/312258>.]
- Wallace, J. M., Tibaldi, S., & Simmons, A. J. (1983). Reduction of systematic forecast errors in the ECMWF model through the introduction of an envelope orography. *Quarterly Journal of the Royal Meteorological Society*, 109(462), 683–717.
- 955 <https://doi.org/10.1002/qj.49710946202>
- Wexler, H.: Cooling in the lower atmosphere and the structure of polar continental air, *Mon. Weather Rev.*, 64, 122–136, [https://doi.org/10.1175/1520-0493\(1936\)64<122:CITLAA>2.0.CO;2](https://doi.org/10.1175/1520-0493(1936)64<122:CITLAA>2.0.CO;2), 1936.
- Wilkinson, M., Dumontier, M., Aalbersberg, I. et al. The FAIR Guiding Principles for scientific data management and stewardship. *Sci Data* 3, 160018 (2016). <https://doi.org/10.1038/sdata.2016.18>
- 960 Zängl, G., Reinert, D., Rípodas, P., and Baldauf, M.: The ICON (ICOsahedral Non-hydrostatic) modelling framework of DWD and MPI-M: Description of the non-hydrostatic dynamical core, *Q. J. R. Meteorol. Soc.*, 141, 563–579, <https://doi.org/10.1002/qj.2378>, 2015.

965